RANGE CALCULATION FOR HEAVY IONS IN COMPLEX MEDIA AND A COULOMETRIC METHOD FOR EXPERIMENTAL RANGE MEASUREMENT

A Thesis Submitted
In Partial Fulfilment of the Requirements
for the Degree of
DOCTOR OF PHILOSOPHY

By

A. KRISHNA NAYAK

to the
DEPARTMENT OF CHEMISTRY
INDIAN INSTITUTE OF TECHNOLOGY, KANPUR
MARCH, 1980

STATEMENT

I hereby declare that the matter embodied in this thesis is the result of investigations carried out by me in the Department of Chemistry, Indian Institute of Technology, Kanpur, India, under the supervision of Professor Shankar Mukherji.

In keeping with the general practice of reporting scientific observations, due acknowledgement has been made wherever the work described is based on the findings of other investigators.

A. Krishna Nayak

Kanpur
March 1980.

DEPARTMENT OF CHEMISTRY,
INDIAN INSTITUTE OF TECHNOLOGY KANPUR, INDIA

CERTIFICATE I

This is to certify that Mr. A. Krishna Nayak has satisfactorily completed all the courses required for the Ph.D. degree programme. These courses include:

Chm 501	Advanced Inorganic Chemistry I
Chm 521	Chemical Binding
Chm 523	Chemical Thermodynamics
Chm 524	Modern Physical Methods
Chm 534	Electronics for Chemists
Chm 541	Advanced Inorganic Chemistry I
Chm 542	Advanced Inorganic Chemistry II
Chm 543	Nuclear Chemistry
Chm 600	Mathematics for Chemists
Chm 650	Statistical Methods and its Applications to Chemistry
Chm 800	General Seminars
Chm 801	Graduate Seminars
Chm 900	Post-Graduate Research

Mr. A. Krishna Nayak was admitted to the candidacy of the Ph.D. degree in October 1975, after he successfully completed the written and oral qualifying examinations.

(S. Ranganathan)
Head,
Department of Chemistry

(D.N. Dhar)
Convener,
Departmental Post-Graduate
Committee

CERTIFICATE II

Certified that the work contained in this thesis, entitled "RANGE CALCULATION FOR HEAVY IONS IN COMPLEX MEDIA AND A COULOMETRIC METHOD FOR EXPERIMENTAL RANGE MEASUREMENT" has been carried out by Mr. A. Krishna Nayak under my supervision and the same has not been submitted elsewhere for a degree.

Shankar Mukherji
Thesis Supervisor

Kanpur
March 1980.

ACKNOWLEDGEMENTS

I owe special gratitude to Professor Shankar Mukherji for his guidance during the course of this work.

I am deeply obliged to Dr. M.V. Ramaniah, Head, Radiochemistry Division, and Dr. R.H. Iyer of Radiochemistry Division, B.A.R.C. (Bhabha Atomic Research Centre), Bombay, for generously making available the neutron irradiation facilities. It is always a great pleasure to remember the help and hospitality extended to me by Drs. R.H. Iyer, A. Ramaswamy and Brijesh K. Srivastava, during my stay at B.A.R.C.

I wish to record my heartfelt thanks to Professors Sudhir Sen and G.K. Mehta of Physics Department and Professors P.S. Goel and S.S. Katiyar of Chemistry Department, Indian Institute of Technology, Kanpur, without whose generous cooperation the experimental work would not have been possible.

My thanks and appreciation are also due to Mr. R.D. Singh of Chemistry Department for the excellent typing, and to Mr. B.K. Jain of A.C.M.S., for the neat drawings.

It is difficult to acknowledge many friends who have helped me in numerous ways, and I hope, the absence of formal acknowlledgement will not be taken to imply absence of gratitude.

A. Krishna Nayak

PREFACE

This thesis entitled "Range Calculation for Heavy Ions in Complex Media and a Coulometric Method for Experimental Range Measurement" deals (a) A theoretical deduction of stopping-power equations for heavy ions in complex media for known molecular formula and (b) Application of coulometry in experimental measurement of ranges of fission products in copper.

Chapter 1 explains the aims and the necessity of the present work in terms of the earlier related work by other workers.

Chapter 2 briefly deals with the energy-loss mechanisms which cause an initially energetic charged particle to slow down inside any medium in terms of Bohr's theory.

Chapter 3 describes the theoretical calculation of the energy-loss and the ranges of heavy ions in complex media like nuclear emulsion. It also gives a new empirical method of calculating the mean ionization potential for any elemental medium.

In Chapter 4 the various general experimental procedures employed for the range determination of heavy ions and fission products are described.

Chapter 5 presents the coulometric method used in the present work for the differential range measurement of the fission products ^{89}Sr, ^{95}Zr and ^{140}Ba in metallic copper.

CONTENTS

		Page
CHAPTER 1 -	Introduction	1
CHAPTER 2 -	Theoretical Aspects of Stopping Process	5
	2.1 Energy loss process	5
	3.2 Electronic stopping process	7
	3.3 Nuclear collisions	18
CHAPTER 3 -	Calculation of Heavy Ion Ranges in Nuclear Emulsion and Other Complex Media	21
	3.1 Introduction	21
	3.2 Derivation of stopping-power equations	22
	3.3 Hydrogen as the stopping medium	34
	3.4 Stopping-power equations	36
	3.5 Mean ionization potential	39
	3.6 Calculation of the ion charge	47
	3.7 Range computations	48
	3.8 Results and discussion	51
CHAPTER 4 -	Techniques of Range Measurements	71
	4.1 Range concepts	71
	4.2 Recoil techniques	72
	4.3 Nuclear emulsions	76
	4.4 Sectioning techniques	78
CHAPTER 5 -	Coulometric Method of Range Measurement	82
	5.1 Introduction	82
	5.2 Target preparation	83
	5.3 Target arrangement and irradiation	85

...contd.

Contents (contd.)

		Page
	5.4 Removal of thin layers from the catcher foil	86
	5.5 Radiochemical separation of fission products and counting	95
	5.6 Results	104
	5.7 Sources of error in the measurement	115
	5.8 Discussion	117
CHAPTER 6 -	Summary	123
APPENDIX	.. ..	125
REFERENCES	.. ..	126

-*-

CHAPTER 1

INTRODUCTION

Theoretical calculation of the energy-loss of energetic charged particles in matter has been one of the important unsolved problems in the realm of physics for a long period of time. In 1913, Niels Bohr[1] first formulated the method of solving it by a purely classical method and was followed by Bethe[2] who used a quantum mechanical approach. In 1948, Bohr[3] looked afresh at the problem in detail and gave a solution which was consistent with his earlier treatment[1] as well as with Bethe's[2] quantum mechanical formulation. However, the stopping-power equation of Bohr[3] contained some summations, the evaluation of which could not be done by any rigorous theoretical procedure. In an approximate manner these are obtainable from a knowledge of the velocity-distribution among the orbital electrons in an atom. In the case of a heavy ion ($Z > 40$) penetrating a heavy medium ($Z > 40$), Bohr[3] himself suggested the use of the Thomas-Fermi statistical approach

for this purpose. For comparatively lighter ions penetrating light media, no statistical approach is suitable so that even a simple approximation is theoretically ruled out. Mukherji and Srivastava,[4] using a semi-empirical approach, showed a way of making Bohr's[3] equation practically useful in the case of partially-stripped heavy ions like fission products and similar accelerated heavy ions. Later they[5] tried to extend it to the case of heavy ions which are almost completely stripped because of their very high velocity. Although, in general, the stopping-power equations deduced by these authors[5] predicted ranges and energy-loss of heavy ions in elemental media, which were in good agreement with the corresponding experimental values, there were some notable exceptions. The present work, in part, deals with an investigation of the reasons of the disagreement between the calculated and the experimental values in the case of some elemental media. After locating the reasons and making suitable modification in the computational procedure, the stopping-power equations have been used for the calculation of ranges of heavy ions in complex media like mylar, polyethylene, tissue material and nuclear emulsion. Although nuclear emulsions have been used for charged-particle identification from the lengths of the tracks, there has been no appropriate, even semi-empirical, general equations relating the track lengths to the velocity of a charged particle of known mass and atomic numbers. The available track-length versus energy equation of Heckman et al.[6] is based on many dubious and arbitrary assumptions. The most serious

drawback of the equation is that it is of an "ad hoc" character. The method used in this work has been step-wise. The equations developed by Mukherji and Srivastava[4] and Srivastava and Mukherji[5] for stopping-power calculations were first modified so that there was good general agreement between the experimental energy-loss in elemental media measured by other authors and those calculated by these equations, without any exception. In the next step, energy-loss in relatively simple compound media like mylar and polyethylene were calculated, using Bragg's additivity rule. This rule assumes that the heavy ion sees no chemical binding in the compound medium and the stopping-power of the compound medium is the sum of the stopping-powers of the constituent elements, weighted according to the number of atoms of each consituent per molecule. The ranges of heavy ions in these media have been computed from the stopping-powers obtained in the aforesaid way. After good agreement was obtained between the experimental and calculated values in those cases, ranges in nuclear emulsion were computed using two different approaches, both leading to practically the same final values.

The other part of the present work consists of testing a new experimental technique for measuring the ranges or depth of penetration of fission products or of similar heavy ions in copper. Of the two general methods[7] of range determination (i.e., "integral and "differential") the differential method requires removal of very thin layers of the "catcher" material and subsequent determination of the concentration of the heavy ion in the layers by

suitable methods like counting of radioactivity. Although it is well-known that metals like copper and silver dissolve quantitatively when used as an anode in an electrolytic cell, no attempts have been made to apply this principle for differential range measurement. In this work, the conditions for dissolving uniformly thin layers of copper has been investigated. The agreement between the experimental and calculated ranges has been quite good, indicating that the electrolytic method may possibly be applied in the case of other metals similar to copper.

The results of the present theoretical and experimental investigations have already been reported in a journal.*

---

* 1. Nucl. Instm. and Methods, 159, 421 (1979).

2. Nucl. Instm. and Methods (accepted) (as part of the Proceedings of the 8th International Conference on Atomic Collisions in Solids).

CHAPTER 2

THEORETICAL ASPECTS OF STOPPING PROCESS

2.1 ENERGY LOSS PROCESSES

The mechanism of energy loss of an energetic charged particle involves four different types of collisions with matter through which it passes.[8]

2.1.1 Inelastic collision with atomic electrons

For swiftly moving charged particles, inelastic collisions with bound atomic electrons of the medium being penetrated is the most important energy loss process. The atomic electrons experience a transition to an excited state (excitation) or to an unbound state (ionization).

2.1.2 Elastic collision with the atomic nucleus

In this type of interaction, also called nuclear collision, the incident particle gets scattered in the screened field of the

nucleus of the stopping atom. During the process the kinetic energy and the momentum are conserved. Nuclear collisions become predominant at low ion-velocities, $\sim 2.2 \times 10^8$ cm/sec.

2.1.3 Inelastic collision with the nucleus

In a close non-capture encounter with the nucleus of the stopping atom the incident charged particle experiences a deflection. In some, but not all such deflections, a quantum of radiation is emitted and a corresponding amount of kinetic energy is lost by the incident charged particle. Since the cross-section for this type of emission is inversely proportional to the mass of the charged particle, this process is not important in the case of heavy charged particles.[8]

2.1.4 Elastic collision with the atomic electrons

The incident charged particle can suffer an elastic collision with the electrons of the struck atom. Both kinetic energy and the momentum are conserved, and the energy transfer is less than the lowest ionization potential of the bound electrons so that the interaction is really with the atom as a whole. This type collision is important only in the case of very low energy electrons as projectiles.

All the four energy-loss processes described above can contribute to the energy loss suffered by the incident particle. Their relative contributions, however, depend upon the energy and the type (heavy or light) of the charged particle. For heavy

charged particles, inelastic collisions with the atomic electrons of the stopping medium, also called electronic collisions, dominate at high ion velocities, while at low velocities, of the order of the most loosely bound atomic electrons of the stopping medium, only nuclear collisions are important.

2.2 ELECTRONIC STOPPING PROCESSES

A brief account of the various electronic stopping equations is given in this section.

2.2.1 Bohr's classical stopping power formula

A detailed discussion of the interaction between a moving charged particle and an electron of the stopping medium was given by Bohr[1] in 1913. Using nonrelativistic classical mechanics and Rutherford's model of the atom, Bohr obtained the following equation for $\frac{dE}{dX}$, the energy loss per unit path length due to electronic collisions:

$$-\frac{dE}{dX} = \frac{4\pi z^2 e^4}{mV^2} n \sum_{s=1}^{s=Z_2} \ln \frac{1.123\ mV^3}{ze^2\ \omega_s} \qquad \ldots(2.1)$$

where ze is the ionic charge of the incident particle, Z_2 is the atomic number of the medium, n is the number of atoms per unit volume of the stopping medium, m and e are the mass and charge of the electron respectively, V is the ion velocity, and ω_s is the cyclic frequency of the s^{th} orbital electron of the stopping atom. The sum includes all the orbital electrons of the stopping

atom. Eq. (2.1) can also be written as

$$-\frac{dE}{dX} = \frac{4\pi z^2 e^4}{mV^2} n Z_2 \ln \frac{1.123\ mV^3}{ze^2\ \bar{\omega}} \tag{2.2}$$

where $\bar{\omega}$ is the geometric mean cyclic frequency of the orbital electrons of the stopping atom, given by

$$Z_2 \ln \bar{\omega} = \sum_{s=1}^{Z_2} \ln \omega_s \tag{2.3}$$

2.2.2 Bethe's stopping power formula

The first purely quantum mechanical treatment of energy loss of charged particles due to electronic collisions was given by Bethe[2] based on the Born approximation. The use of the Born approximation requires that

$$\frac{ze^2}{\hbar V} << 1 \tag{2.4}$$

where ze and V are the charge and the velocity of the charged particle. This condition is usually satisfied at high velocities and small charges of the moving particle. Under these conditions the non-relativistic stopping-power formula is given by[2]

$$-\frac{dE}{dX} = \frac{4\pi z^2 e^4}{mV^2} n Z_2 \ln \frac{2\ mV^2}{I} \tag{2.5}$$

where I is the mean excitation potential for the atoms of the

stopping medium. For relativistic velocities of the charged particle the energy-loss is given by

$$-\frac{dE}{dX} = \frac{4\pi z^2 e^4}{mV^2} n Z_2 \left\{\ln \frac{2mV^2}{I(1-\beta^2)} - \beta^2\right\} \qquad (2.6)$$

where $\beta = \frac{V}{c}$, and c is the velocity of light.

2.2.3 Bloch's equation

The condition for the validity of the Born approximation, $\frac{ze^2}{\hbar V} << 1$, and the classical approximation, $\frac{ze^2}{\hbar V} >> 1$, are complementary to each other.[3] A bridge between Bohr's equation and Bethe's equation was provided by Bloch[9] who took into consideration the perturbation of wave functions the atomic electrons of the stopping atom in the presence of a charged particle. The non-relativistic stopping-power formula due to Bloch[9] is

$$-\frac{dE}{dX} = \frac{4\pi z^2 e^4}{mV^2} n Z_2 \left\{\ln \frac{2mV^2}{I} + \psi(1) - R\psi\left(1 + i\frac{ze^2}{\hbar V}\right)\right\} \qquad (2.7)$$

where ψ is the logarithmic derivative of the gamma function and $R\psi$ denotes the real part of ψ. For $\frac{ze^2}{\hbar V} >> 1$ Eq. (2.7) reduces[3] to Eq. (2.2) and for $\frac{ze^2}{\hbar V} << 1$ it reduces to Bethe's formula, Eq. (2.5). For intermediate values of $\frac{ze^2}{\hbar V}$, Eq. (2.7) is approximately identical with Eq. (2.2) or Eq. (2.5).

Bloch[9] made another interesting contribution by showing that for atoms which can be adequately described using the

Thomas-Fermi statistical model, the mean excitation potential I is proportional to the atomic number Z_2;

$$I = k\, Z_2 \tag{2.8}$$

The "Bloch constant" k has to be determined experimentally.

2.2.4 Bohr's semi-quantum mechanical treatment of electronic collisions

The classical equation of Bohr and the quantum mechanical equation of Bethe are based on the conditions that $\chi >> 1$ and $\chi << 1$, respectively, were χ is given by

$$\chi = 2\, z\, \frac{V_o}{V} \tag{2.9}$$

In Eq. (2.9) z is the charge of the ion in units of the electronic charge e, V is the ion velocity, and $V_o = \frac{e^2}{\hbar}$. That the two equations predict the same energy-loss for $\chi = 1$ is, in a sense, accidental, since they are derived for values of χ which are mutually exclusive.[3]

In 1948 Bohr[3] attempted a more detailed analysis of the problem using a semi-classical approach. A brief derivation of these stopping power equations is given below:

When a swift charged particle is penetrating matter the loss in kinetic energy will be primarily due to collisions with the atomic electrons of the penetrated medium. The collisions can be divided into two types, namely, "free collisions" and "resonance collisions".

Free collisions- When the time of interaction between the charged particle and the electron of the stopping atom is very small compared to the period of oscillation of the electron in the atom, to a first approximation, the influence of the atomic binding forces can be neglected and the electron can be considered as free. Such collisions are called "free collisions." Free collisions are accompanied by ionization and excitation of the medium.

Resonance collisions- When the time of interaction between the charged particle and an electron is very large compared to the period of oscillation of the electron in the atom, the field exerted by the moving charged particle will be practically uniform over the entire atomic region. This type of collisions are called "resonance collisions".

The ionization potential of the s^{th} electron, I_s, is given by

$$I_s = \frac{1}{2} m U_s^2 , \tag{2.10}$$

where U_s is the velocity of the s^{th} electron of the stopping medium, and m is the electron mass. If the length a_s is defined by

$$a_s = \frac{\hbar}{mU_s} , \tag{2.11}$$

then a_s is a measure of the radius of the orbit of the s^{th} electron. In quantum mechanical terminology, mU_s can be

considered[3] as the expectation value of the momentum of the electron and a_s as the accuracy with which the electron can be localized without the uncertainty in its energy exceeding I_s. If ω_s is the cyclic frequency of the s^{th} electron, the ionization potential, I_s, can also be written as

$$I_s = \hbar \omega_s \qquad (2.12)$$

As pointed out earlier, the problem of electronic collision effects produced by fast moving particles depends essentially on the value of the quantity χ . Hence, it is convenient to treat the two cases $\chi > 1$ and $\chi < 1$ separately.

$\chi > 1$

The classical orbital picture of the electrons can be used to describe the individual encounters between the particle and the atomic electron.[3] The collision time, τ , for coulombic interaction for such systems is given by $\tau \approx p/V$, where p is the impact parameter. For this to be of the order of the period of oscillation of the atomic electron, the impact parameter $p = d_s$ is given by

$$p = \frac{V}{\omega_s} \quad , \qquad (2.13)$$

where ω_s is cyclic frequency of the s^{th} electron.

The energy transfer, T, to a free electron by a charged particle for an impact parameter p is obtained from the relation

$$T = \frac{2 z^2 e^4}{mV^2} \quad \frac{1}{p^2} \tag{2.14}$$

If $p = i_s$ is the impact parameter for which $T = I_s$, the ionization potential of the s^{th} electron,

$$i_s = b \frac{V}{U_s} , \tag{2.15}$$

where the collision diameter, b, which is the shortest possible distance of approach in a head-on collision between the electron and the incident particle is given by

$$b = \frac{2 ze^2}{mV^2} . \tag{2.16}$$

When $V >> U_s$, $d_s >> a_s$ and $a_s > b$, d_s can be taken as the effective adiabatic limit, and for impact parameters greater than d_s the energy-loss will be negligibly small, and as a first approximation can be neglected.

Using Eqs. (2.10), (2.11) and (2.12) d_s can be written as

$$d_s = \frac{V}{\omega_s} = \eta_s a_s , \tag{2.17}$$

where a new parameter η_s defined by

$$\eta_s = \frac{2V}{U_s} , \tag{2.18}$$

has been introduced. Using Eqs. (2.15) and (2.17) one obtains

$$\frac{d_s}{i_s} = 2\frac{a_s}{b} = \eta_s \chi^{-1} \tag{2.19}$$

For $\eta_s > \chi$, i_s is always less than d_s and the collisions with impact parameters $p < i_s$ may be considered as free and the energy transfer T will be always greater than the ionization potential, I_s. The energy-loss due to free collisions is given by

$$(\Delta E_s)_f = n \cdot \Delta X \cdot B_\varepsilon \ln\{(\frac{T_m}{I_s})\} \tag{2.20}$$

In Eq. (2.20) T_m is the maximum energy transfer to the electron and is equal to $2mV^2$, n is the number of atoms per unit volume of the stopping medium, ΔX is the distance traversed by the charged particle, and B_ε is defined by

$$B_\varepsilon = \frac{2\pi z^2 e^4}{mV^2} \tag{2.21}$$

Substituting the value of I_s and T_m, Eq. (2.20) can be written as

$$(\Delta E_s)_f = n \cdot \Delta X \cdot B_\varepsilon \ln\{\frac{2V}{U_s}\}^2$$

$$= n \cdot \Delta X \cdot B_\varepsilon \ln \eta_s^2 . \tag{2.22}$$

For $i_s > a_s$, the encounters with $p > i_s$ are of a simple resonance type. The contribution to energy loss due to resonance collisions is given by

$$(\Delta E_s)_r = n \cdot \Delta X \cdot B_\varepsilon \ln \frac{I_s}{D_s} , \qquad (2.23)$$

where D_s is the energy transfer corresponding to impact parameter d_s. Substituting the values of I_s and D_s from Eq. (2.10) and (2.14), and expressing the logarithmic arguments in terms of η_s and χ one obtains

$$(\Delta E_s)_r = n \cdot \Delta X \cdot B_\varepsilon \ln (\eta_s^2 \chi^{-2}). \qquad (2.24)$$

If $\chi > \eta_s$, in which case $i_s > d_s$, the values of p for which the collisions can be considered 'free' no longer extend to i_s since for $p > d_s$ the duration of the encounter exceeds $1/\omega_s$. On the otherhand, all collisions for which $p > d_s$ will not be of a purely adiabatic type. According to Bohr[3] the limiting value d_s^* of the impact parameter for which the probability of ionization can still be assumed to be unity is given by

$$(d_s^*)^2 = i_s \cdot d_s . \qquad (2.25)$$

If D_s^* is the energy transfer corresponding to the impact parameter $p = d_s^*$, the energy-loss due to free collisions is given by

$$(\Delta E_s)_f = n \cdot \Delta X \cdot B_\varepsilon \ln (T_m / D_s^*)$$

$$= n \cdot \Delta X \cdot B_\varepsilon \ln (\eta_s^3 \chi^{-1}) , \qquad (2.26)$$

holding for $T_m >> D_s^*$ or $\chi << \eta_s^3$. The total energy-loss to the s^{th} orbital electron E_s due to free collisions and resonance effects will be the sum of Eqs. (2.22), (2.24) and (2.26).

$$\Delta E_e = n \cdot \Delta X \cdot B_\varepsilon \left\{ \ln \eta_s^2 \chi^{-2} + \ln \eta_s^2 \left[\frac{\chi}{\eta_s} \right]^{-1} \right\} \qquad (2.27)$$

where the quantity inside the square bracket, if less than unity, should be replaced by unity.

$\chi < 1$

For $\chi < 1$ the orbital picture of classical mechanics completely fails in accounting for individual collision effects. However, for $\chi < 1$ the separation between the "free" and "resonance" collisions is possible[3] to a first approximation, and these correspond to $p < a_s$ and $p > a_s$ respectively. The energy-loss due to free collisions is still given by Eq. (2.20) while that for resonance effects is given by

$$(\Delta E_s)_r = n \cdot \Delta X \cdot B_\varepsilon \ln \frac{A_s'}{D_s} , \qquad (2.28)$$

where A_s' is the energy transfer calculated according to classical mechanics for $p = a_s$. On substituting the values of A_s' and D_s, and simplification, one obtains

$$(\Delta E_s)_r = n \cdot \Delta X \cdot B_\varepsilon \ln \eta_s^2 . \qquad (2.29)$$

Thus, for $\chi < 1$, the total energy-loss, E_s, to the s^{th} orbital electron of the stopping medium is given by

$$\Delta E_s = (\Delta E_s)_f + (\Delta E_s)_r$$

$$= 2\,n \cdot \Delta X \cdot B_\varepsilon \ln \eta_s^2 \,. \qquad (2.30)$$

A comprehensive energy-loss equation can be written[3] by combining Eqs. (2.27) and (2.30):

$$-\frac{\Delta E}{\Delta X} = n \cdot B \sum_s \ln \eta_s^2 [\chi]^{-2} + \sum_s \ln \{\eta_s^2 \left[\frac{\chi}{\eta_s}\right]^1\} \,, \qquad (2.31)$$

where the terms within the square brackets if less than unity are to be replaced by unity, and the summation is to be carried over all orbital electrons which interact with the moving charged particle. $(\frac{\Delta E}{\Delta X})$, the rate of energy-loss per unit path length, is called the stopping power of the medium for the charged particle concerned.

2.2.5 LSS THEORY

In 1963 Lindhard *et al.*[10] worked out a theory for energy-loss of swiftly moving charged particles based on the Thomas-Fermi model of the atom and the theory of quasielastic collisions between the charged particle and the atoms of the stopping medium. According to this theory the electronic stopping-cross section, S_e per atom[10] is given by

$$S_e = \xi\, 8\pi e^2 a_o \frac{Z_1 Z_2}{(Z_1^{2/3} + Z_2^{2/3})^{1/2}} \frac{V}{V_o} \qquad (2.32)$$

holding for the velocities of the charged particle, $V < Z_1^{2/3} V_o$. In Eq. (2.32), Z_1 and Z_2 are the atomic numbers of the charged particle and the stopping medium respectively, a_o and V_o are the radius and the velocity of the electron in the first Bohr orbit of the hydrogen atom, e is the electronic charge, and ξ is of the order of $Z_1^{1/6}$.

2.3 NUCLEAR COLLISIONS

The coulomb interaction between the screened nuclear charges of the incident charged particle and the atoms of the stopping medium, often referred to as "nuclear collision" becomes the dominant mechanism of energy-loss only when the velocity of the charged particle becomes less than the velocity of the most loosely bound electrons of the stopping atom. It is simply Rutherford scattering between two charged nuclei modified by proper screening by charge clouds of the orbital electrons.

In terms of energy transfer, T, the Rutherford differential cross-section $d\sigma$ for collision between two particles carrying charges $q_1 e$ and $q_2 e$ is given by

$$d\sigma\,(E,T) = \frac{2\pi q_1^{\,2} q_2^{\,2} e^4}{m_2 V^2} \frac{dT}{T^2} = \frac{\pi q_1^{\,2} q_2^{\,2} e^4}{E} \left(\frac{M_1}{M_2}\right) \frac{dT}{T^2}\,, \qquad (2.33)$$

where E is the kinetic energy of the incident particle in the laboratory co-ordinates, and M_1 , M_2 are the masses of the incident and struck particles respectively. In the case of a collision between a low-velocity heavy ion and an atom of the stopping medium the presence of the bound atomic electrons causes shielding of the nuclear charge and hence the interaction potential has to be suitably modified. The exponential screening potential due to Bohr[3] between two atoms with nuclear charges Z_1e and Z_2e is given by

$$V(r) = \frac{Z_1 Z_2 e^2}{r} e^{-r/a_s} \qquad (2.34)$$

where 'a_s' is the screening parameter defined by

$$a_s = \frac{a_o}{(Z_1^{2/3} + Z_2^{2/3})^{\frac{1}{2}}} . \qquad (2.35)$$

The applicability of Rutherford's equation depends on the ratio ζ between 'a_s' and the collision diameter 'b' for an unscreened field: $\zeta = b/a$. If $\zeta \ll 1$ and $\chi \gg 1$, the interaction will be confined mostly to the unscreened part of the field.[3] For strong screening, i.e., $\zeta \gg 1$, the collisions may be considered as occurring between two rigid spheres, the radii of the spheres will, however, depend upon the energy of the incident particle. Taking these factors into consideration and using Rutherford's

scattering theory, Bohr[3] derived an expression for the rate of energy-loss due to nuclear collisions:

$$-\frac{dE}{dX} = \frac{2\pi Z_1^2 Z_2^2 e^4}{M_2 V^2} n \ln\left(\frac{M_1 M_2}{M_1 + M_2} \cdot \frac{V^2 a_s}{Z_1 Z_2 e^2}\right), \qquad (2.36)$$

where a_s is the screening parameter defined earlier.

CHAPTER 3

CALCULATION OF HEAVY ION RANGES IN NUCLEAR EMULSION AND OTHER COMPLEX MEDIA

3.1 INTRODUCTION

The stopping-power equations, one due to Bohr[1] and the other due to Bethe,[2] have their restricted regions of validity.[3,11] Recently, starting with the classical stopping-power formula due to Bohr,[3] Srivastava and Mukherji[5] deduced a set of stopping-power equations for calculating the electronic stopping-powers of heavy ions at all ion velocities greater than $e^2/\hbar$. While these equations predicted stopping-powers and ranges quite well for fission fragments and heavy ions in light stopping media (i.e., atomic numbers less than 14), considerable disagreements were observed in the case of heavier media. This necessitated a reinvestigation of these stopping-power equations.

3.2 DERIVATION OF STOPPING POWER EQUATIONS

The energy-loss per unit path length dE/dX for a heavy ion of ionic charge ze and velocity V due to electronic collision has been given by Bohr:[3]

$$\frac{dE}{dX} = \frac{2\pi z^2 e^4 n}{mV^2} \{ \sum_s \ln\left(\eta_s^2 \left[\chi\right]^{-2}\right) + \sum_s \ln\left(\eta_s^2 \left[\frac{\chi}{\eta_s}\right]^{1}\right)\} , \qquad (3.1)$$

where n is the number of atoms of the medium per unit volume, e and m are the charge and the mass of the electron. χ and η_s are defined by

$$\chi = 2z \frac{V_o}{V} , \qquad (3.2)$$

$$\eta_s = \frac{2V}{U_s} , \qquad (3.3)$$

where U_s is the velocity of the s^{th} orbital electron of the stopping atom, and $V_o = e^2/\hbar$. In Eqn. (3.1) the quantities within the square brackets, if less than 1, should be replaced by unity.[3] Using this condition and the definitions of χ and η_s, the second term in Eq. (3.1) can be split into two terms as follows:

Since, $\frac{\chi}{\eta_s} = \frac{U_s}{2V\ \chi^{-1}}$,

for $U_s < 2V\ \chi^{-1}$, $\frac{\chi}{\eta_s} < 1$ and for $U_s > 2V\ \chi^{-1}$, $\frac{\chi}{\eta_s} > 1$. Hence,

$$\sum_s \ln\left(\eta_s^2 \left[\frac{\chi}{\eta_s}\right]^{-1}\right) = \sum_{U_s=0}^{U_s=2V\ \chi^{-1}} \ln \eta_s^2 + \sum_{U_s=2V\ \chi^{-1}}^{U_s=U_s''} \ln(\eta_s^3\ \chi^{-1}) \qquad (3.4)$$

Therefore Eq. (3.1) can be written as

$$\frac{dE}{dX} = \frac{2\pi z^2 e^4 n}{mV^2}\left\{ \sum_{U_s=0}^{U_s=U_s'} \ln\left(\eta_s^2 [\chi]^{-2}\right) + \sum_{U_s=0}^{U_s=2V\chi^{-1}} \ln \eta_s^2 + \sum_{U_s=2V\chi^{-1}}^{U_s=U_s''} \ln\left(\eta_s^3 \chi^{-1}\right)\right\} \tag{3.5}$$

where U_s' and U_s'' are the upper cut-off velocities[3,5] which render the logarithmic terms zero conforming to the fact that physically no negative energy-loss is possible. For convenience Eq. (3.5) will be written as

$$\frac{dE}{dX} = \frac{2\pi z^2 e^4 n}{mV^2}\left(J_1 + J_2 + J_3\right) \tag{3.6}$$

where

$$J_1 = \sum_{U_s=0}^{U_s=U_s'} \ln\left(\eta_s^2 [\chi]^{-2}\right), \tag{3.7}$$

$$J_2 = \sum_{U_s=0}^{U_s=2V\chi^{-1}} \ln \eta_s^2, \tag{3.8}$$

$$J_3 = \sum_{U_s=2V\chi^{-1}}^{U_s=U_s''} \ln\left(\eta_s^3 \chi^{-1}\right), \tag{3.9}$$

and, further, the sum of the three terms J_1, J_2 and J_3 will be represented by S,

$$S = J_1 + J_2 + J_3 \ . \qquad (3.10)$$

In Eq. (3.5) the summation terms, as Bohr[3] showed, could be replaced by integrals if the velocity distribution function for the orbital electrons were known. As a first approximation, for atoms which can be adequately described using the Thomas-Fermi statistical model, Bohr[3] gave the following formula for $n(U_s)$:

$$n(U_s) = Z^{1/3} \frac{U_s}{V_o} \qquad (3.11)$$

where $n(U_s)$ is the number of orbital electrons with velocity less than U_s for $V_o < U_s < Z\ V_o^{2/3}$. Z is the atomic number of the atom. For light atoms, which are not expected to obey the Thomas-Fermi statistical model Eq. (3.11) is not valid. Various empirical estimates for $n(U_s)$ have been made.[4] In the present work an empirical formula

$$n(U_s) = f(Z) \frac{U_s}{V_o} \qquad (3.12)$$

with $f(Z) = 0.3634\ Z^{0.555}$ has been used (cf. Section 3.5).

In order to obtain a set of general stopping-power equations it is necessary to evaluate the summation terms corresponding to different physical conditions determined by χ, z, V and the atomic number of the stopping medium, Z_2. The two cases $\chi > 1$ and $\chi < 1$ are treated separately for convenience.

$\chi > 1$

i) $V \geq \frac{1}{2} Z_2 V_o \chi$

J_1 can be written as

$$J_1 = \sum_{U_s=0}^{U_s=U_s'} \ln (\eta_s^2 \chi^{-2}) = \sum_{U_s=0}^{U_s=U_s'} \ln (2V/U_s \chi)^2 \qquad (3.13)$$

Since the logarithmic term remains positive for all values of U_s from $U_s=0$ to $U_s=2V \chi^{-1} = Z_2 V_o$, the summation between the limits $U_s = 0$ to $U_s=U_s'$ is equivalent to the inclusion of all the Z_2 electrons of the stopping atom. The velocity of the K-shell electrons of the medium of atomic number Z_2 is taken as $Z_2 V_o$. Since η_s can be written as

$$\eta_s^2 = \left(\frac{2V}{U_s}\right)^2 = \frac{2mV^2}{\frac{1}{2} mU_s^2}$$

$$= \frac{2mV^2}{I_s} \qquad (3.14)$$

where I_s is the ionization potential of the s^{th} orbital electron, for J_1 one obtains

$$J_1 = \sum_{s=1}^{s=Z_2} \ln \frac{2mV^2}{I_s \chi^2}$$

$$= Z_2 \ln \frac{2mV^2}{\bar{I} \chi^2} \qquad (3.15)$$

where $\bar{I}$ is the geometric mean ionization potential of the atoms of the stopping medium, and is defined by the equation

$$Z_2 \ln \bar{I} = \sum_{s=1}^{s=Z_2} \ln I_s \, . \qquad (3.16)$$

Since $V \geqslant \frac{1}{2} Z_2 V_o \chi$ has been set as the upper limit, for J_2 one obtains

$$J_2 = \sum_{U_s=0}^{U_s=2V\chi^{-1}} \ln \eta_s^2 = \sum_{U_s=0}^{U_s=Z_2V_o} \ln (2V/U_s)^2$$

$$= \sum_{s=1}^{s=Z_2} \ln (2mV^2/I_s)$$

$$= Z_2 \ln (2mV^2/\bar{I}) \, . \qquad (3.17)$$

Since the lower limit of U_s in J_3 corresponds to the maximum possible value of U_s, J_3 becomes redundant. Therefore

$$S = J_1 + J_2 + J_3 = 2Z_2 \ln (2mV^2 / \bar{I}\chi) \qquad (3.18)$$

ii) $\dfrac{Z_2V_o\chi}{2} > V > \dfrac{(Z_2-2)V_o\chi}{2f(Z_2)}$

In this case the ion may not be able to ionize all the atomic electrons of the medium. In evaluating the contribution of J_3 term it is useful to replace the summation by integration

using the differential form of $n(U_s)$, viz.,

$$dn(U_s) = f(Z_2) \frac{dU_s}{V_o} . \qquad (3.19)$$

Since the two K-shell electrons of the atom are practically unshielded Mukherji[12] suggested that their contribution to the stopping power can be computed separately. Accordingly, J_3 can be written as

$$J_3 = \int_{2V\,\chi^{-1}}^{\frac{(Z_2-2)V_o}{f(Z_2)}} \ln\left(2V/U_s\,\chi^{1/3}\right)^3 dn(U_s) + 2\ln\left(2V/Z_2V_o\,\chi^{1/3}\right)^3 \qquad (3.20)$$

The upper limit of the first integral stands for the velocity of the $(Z_2-2)^{th}$ orbital electron of the medium as given by Eq. (3.12) and the second term represents the contribution of the two K-shell electrons. Earlier, Srivastava and Mukherji[5] evaluated J_3 in the ion velocity region $\frac{Z_2V_o\chi}{2} > V > \frac{Z_2V_o\,\chi^{1/3}}{2f(Z_2)}$ without considering the possibility of the occurrence of the condition $2V\,\chi^{-1} \geqslant \frac{(Z_2-2)V_o}{f(Z_2)}$. If $2V\,\chi^{-1} \geqslant \frac{(Z_2-2)V_o}{f(Z_2)}$ the integral in Eq. (3.20) becomes zero, and further, if $V \leqslant \frac{Z_2V_o\,\chi^{1/3}}{2}$, J_3 itself becomes zero. Thus the following two cases arise if $\frac{Z_2V_o\chi}{2} > V > \frac{(Z_2-2)V_o}{2\,f(Z_2)}$.

(a) $\underline{V \geqslant \frac{Z_2V_o\chi}{2}}$. In this case

$$J_3 = 2\ln\left(2V/Z_2V_o\,\chi^{1/3}\right)^3 \qquad (3.21)$$

As far as J_1 is concerned since the upper cut-off value U_s' equals $2V\ \chi^{-1}$, and as $2V\ \chi^{-1}$ is greater than the velocity of the $(Z_2-2)^{th}$ electron but less than that of the K-shell electrons, the summation would include only the outer (Z_2-2) electrons. Thus,

$$J_1 = \sum_{U_s=0}^{U_s'=2V\chi^{-1}} \text{on } (\eta_s^2\ \chi^{-2})$$

$$= \sum_{s=1}^{s=Z_2-2} \ln\ (2mV^2/\ I_s\ \chi^2)$$

$$= (Z_2-2)\ \ln\ (2mV^2/\ \bar{I}_1\ \chi^2) \qquad (3.22)$$

where $\bar{I}_1$ is the geometric mean ionization potential of the outer (Z_2-2) electrons of the stopping medium and is given by the relation

$$(Z_2-2)\ \ln\ \bar{I}_1 = \sum_{s=1}^{s=Z_2-2} \ln\ I_s\ . \qquad (3.23)$$

The value of $\bar{I}_1$ has been obtained from Mukherji's formula[12]

$$\bar{I}_1 = 13.6\ \{\frac{Z_2-2}{2.717\ f(Z_2)}\}^2\ . \qquad (3.24)$$

In a similar manner one obtains for J_2

$$J_2 = \sum_{U_s=0}^{U_s=2V\chi^{-1}} \ln\ \eta_s^2 = \sum_{s=1}^{s=Z_2-2} \ln\ (2mV^2/I_s)$$

$$= (Z_2-2)\ \ln\ (2mV^2/\bar{I}_1) \qquad (3.25)$$

Therefore,

$$S = J_1 + J_2 + J_3 = 2(Z_2-2) \ln (2mV^2/\bar{I}_1 \chi) + 2 \ln (2V/Z_2V_o \chi^{1/3})^3 \quad (3.26)$$

(b) $V \leqslant \frac{Z_2V_o \chi^{1/3}}{2}$. In this case J_3 becomes zero, while J_1 and J_2 are given by Eqs. (3.22) and (3.25) respectively. Thus,

$$S = J_1 + J_2 = 2(Z_2-2) \ln (2mV^2/\bar{I}_1 \chi) \quad (3.27)$$

(iii) $\frac{(Z_2-2)V_o}{2f(Z_2)} > V > \frac{Z_2V_o \chi^{1/3}}{2}$

Since $2V \chi^{-1}$ is less than the velocity of the $(Z_2-2)^{th}$ electron, both J_1 and J_2 would require an upper cut-off value of $2V \chi^{-1}$. Therefore, for J_1, J_2 and J_3 one gets

$$J_1 = \sum_{U_s=0}^{U_s=2V\chi^{-1}} \ln (2V \chi^{-1}/U_s) = 2 \int_{U_s=0}^{U_s=2V\chi^{-1}} \ln(2V \chi^{-1}/U_s)\, dn(U_s)$$

$$= \frac{2f(Z_2)}{V_o} \int_{U_s=0}^{U_s=2V\chi^{-1}} \ln (2V \chi^{-1}/U_s)\, dU_s = \frac{4f(Z_2) \chi^{-1} V}{V_o} \quad (3.28)$$

$$J_2 = \sum_{U_s=0}^{U_s=2V\chi^{-1}} \ln (2V/U_s)^2 = 2 \int_{U_s=0}^{U_s=2V\chi^{-1}} \ln (2V/U_s)\, dn(U_s)$$

$$= \frac{2f(Z_2)}{V_o} \int_{U_s=0}^{U_s=2V\chi^{-1}} \ln \left(\frac{2V}{U_s}\right) dU_s = \frac{4f(Z_2) \chi^{-1}(1+\ln \chi)}{V_o} V \quad (3.29)$$

$$U_s = \frac{(Z_2-2)V_o}{f(Z_2)}$$

$$J_3 = \int_{2V\,x^{-1}}^{\frac{(Z_2-2)V_o}{f(Z_2)}} \ln\left\{\left(\frac{2V}{U_s}\,x^{-1/3}\right)^3\right\} dn(U_s) + 2\ln\left\{\left(\frac{2V}{Z_2V_o}\right)^3 x^{-1}\right\}$$

$$= \frac{3f(Z_2)V}{V_o} \int_{2V\,x^{-1}}^{\frac{(Z_2-2)V_o}{f(Z_2)}} \ln\left(\frac{2V}{U_s\,x^{1/3}}\right) dU_s + 2\ln\left(\frac{2V}{Z_2\,x^{1/3}}\right)^3$$

$$= \frac{3f(Z_2)}{V_o}\left\{\frac{(Z_2-2)V_o}{f(Z_2)} - 2V\,x^{-1} + 2V\,x^{-1}\ln x^{-2/3}\right.$$

$$- \frac{(Z_2-2)V_o}{f(Z_2)}\ln\frac{(Z_2-2)V_o\,x^{1/3}}{2V\,f(Z_2)}$$

$$\left. + 6\ln\left(\frac{2V}{Z_2V_o}\right) - 2\ln x\right\} \qquad (3.30)$$

Thus

$$S = J_1 + J_2 + J_3 = 3(Z_2-2) + 3(Z_2-2)\ln\frac{2f(Z_2)V}{(Z_2-2)V_o}$$

$$+ 6\ln\frac{2V}{Z_2V_o} + \frac{2f(Z_2)V}{V_o x} - Z_2\ln x \qquad (3.31)$$

(iv) $\dfrac{Z_2V_o\,x^{1/3}}{2} > V > \dfrac{(Z_2-2)V_o\,x^{1/3}}{2f(Z_2)}$

J_1 and J_2 would be still given by Eqs. (3.28) and (3.29) respectively. As far as J_3 is concerned, since $V < \dfrac{Z_2V_o\,x^{1/3}}{2}$,

the second term on the right hand side in Eq. (3.20) becomes zero. Therefore, for J_3 one obtains

$$J_3 = \int_{2V\ x^{-1}}^{\frac{(Z_2-2)V_o}{f(Z_2)}} \ln\left(\frac{2V}{U_s\ x^{1/3}}\right)^3 dn(U_s)$$

$$= \frac{3f(Z_2)}{V_o}\left\{\frac{(Z_2-2)V_o}{f(Z_2)} - 2V\ x^{-1} + 2V\ x^{-1} \ln\ x^{3/2}\right.$$

$$\left. - \frac{(Z_2-2)V_o}{f(Z_2)} \ln \frac{(Z_2-2)V_o\ x^{1/3}}{2V\ f(Z_2)}\right\} \qquad (3.32)$$

Hence,

$$S = J_1 + J_2 + J_3 = 3(Z_2-2) + \frac{2f(Z_2)V}{V_o x}$$

$$- 3\ (Z_2-2) \ln\left\{\frac{(Z_2-2)V_o\ x^{1/3}}{2V\ f(Z_2)}\right\} \qquad (3.33)$$

(v) $V < \dfrac{(Z_2-2)V_o}{2f(Z_2)}\ x^{1/3}$

In this case J_1 and J_2 are given by Eqs. (3.28) and (3.29) respectively. J_3 requires an upper cut-off value of $U_s'' = 2V\ x^{-1/3}$. Thus, for J_3 one obtains

$$J_3 = \frac{3f(Z_2)}{V_o} \int_{2V\ x^{-1}}^{2V\ x^{-1/3}} \ln\left(\frac{2V}{U_s\ x^{1/3}}\right) dU_s = \frac{-4f(Z_2)V\ x^{-1}}{V_o} \ln\ x^{-1}$$

$$+ \frac{3f(Z_2)}{V_o}\left(2V\ x^{-1/3} - 2V\ x^{-1}\right) \qquad (3.34)$$

and hence

$$S = J_1 + J_2 + J_3 = \frac{2f(Z_2)V}{V_o} (3\ \chi^{-1/3} + \chi^{-1}) \qquad (3.35)$$

$\chi < 1$

For $\chi < 1$

$$J_1 = \sum_{U_s=0}^{U_s=U_s'} \ln \eta_s^2 \quad \text{and} \qquad (3.36)$$

$$J_2 = \sum_{U_s=0}^{U_s=2V\ \chi^{-1}} \ln \eta_s^2 \qquad (3.8)$$

Since $U_s = 2V\ \chi^{-1}$ is greater than the maximum allowable value of $U_s'' = 2V\ \chi^{-1/3}$, for $\chi < 1$, J_3 becomes redundant.

(i) $V > \frac{Z_2 V_o}{2}$

In this case even the K-shell electrons of the medium can be ionized. Therefore, the summation in J_1 and J_2 will be over all the Z_2 atomic electrons.

$$J_1 = J_2 = \sum_{s=1}^{s=Z_2} \ln \left(\frac{2V}{U_s}\right)^2 = 2 \sum_{s=1}^{s=Z_2} \ln (2mV^2/I_s)$$

$$= 2 Z_2 \ln (2mV^2/\bar{I}) \qquad (3.37)$$

Therefore,

$$S = J_1 + J_2 = 4\ Z_2 \ln (2mV^2/\bar{I}) \qquad (3.38)$$

where $\bar{I}$ has been defined already by Eq. (3.16).

(ii) $\frac{Z_2 V_o}{2} > V > \frac{(Z_2-2)V_o}{2f(Z_2)}$

Since $V < \frac{Z_2 V_o}{2}$, the maximum velocity imparted by the particle is less than the orbital velocity of the K-shell electrons. Therefore, the K-shell electrons can not participate in the energy loss process. However, the velocity of the $(Z_2-2)^{th}$ electron is $\frac{(Z_2-2)V_o}{f(Z_2)}$. Therefore all the electrons upto the $(Z_2-2)^{th}$ electron would be ionized. Hence,

$$J_1 = J_2 = \sum_{s=1}^{s=Z_2-2} \ln \left(\frac{2V}{U_s}\right)^2$$

$$= 2 \sum_{s=1}^{s=Z_2-2} \ln \frac{2mV^2}{I_s}$$

$$= 2 (Z_2-2) \ln \frac{2mV^2}{\bar{I}_1} \qquad (3.39)$$

where $\bar{I}_1$ has been already defined by Eq. (3.23).

$$S = J_1 + J_2 = 4(Z_2-2) \ln \frac{2mV^2}{\bar{I}_1} \qquad (3.40)$$

(iii) $V < \frac{(Z_2-2)V_o}{2f(Z_2)}$

This condition requires an upper cut-off value of 2V for U_s.

$$J_1 = J_2 = \sum_{U_s=0}^{U_s=2V} \ln \left(\frac{2V}{U_s}\right)^2 = \frac{2f(Z_2)}{V_o} \int_o^{2V} \ln \left(\frac{2V}{U_s}\right) dn(U_s)$$

$$= \frac{4f(Z_2)V}{V_o} \qquad (3.41)$$

$$S = J_1 + J_2 = \frac{8f(Z_2)V}{V_o} \qquad (3.42)$$

3.3 HYDROGEN AS THE STOPPING MEDIUM

The general stopping power equations derived above for multielectron atoms have to be modified for hydrogen as the stopping medium. Since hydrogen atom has only one orbital electron the summation in Eq. (3.1) becomes redundant and U_s has to be replaced by V_o. Thus,

$$S = \ln \eta_s^2 \left[\chi\right]^{-2} + \ln \{\eta_s^2 \left[\frac{\chi}{\eta_s}\right]^{-1}\}$$

$$= \ln \{(\frac{2V}{V_o})^2 \left[\chi\right]^{-2}\} + \ln \{(\frac{2V}{V_o})^2 \left[\frac{V_o \chi}{2V}\right]^{-1}\} \qquad (3.43)$$

where, as before, the quantity within the square bracket, if less than 1, should be replaced by unity. The two cases $\chi > 1$ and $\chi < 1$ will be treated separately.

$\chi > 1$

In this case S is given by

$$S = \ln (\frac{2V}{V_o})^2 + \ln \{(\frac{2V}{V_o})^2 \left[\frac{V_o \chi}{2V}\right]^{-1}\} . \qquad (3.44)$$

Depending upon the magnitude of the ion velocity two cases arise:

(i) $V > \frac{V_o \chi}{2}$

Under this condition $\frac{V_o \chi}{2} < 1$ and therefore,

$$S = \ln (\frac{2V}{V_o})^2 + \ln (\frac{2V}{V_o})^2 = 2 \ln \frac{2mV^2}{I} \qquad (3.45)$$

where I is the ionization potential of the hydrogen atom.

(ii) $\frac{V_o \chi}{2} > V > \frac{V_o \chi^{1/3}}{2}$

For $\frac{V_o \chi}{2} > V$ the first term in Eq. (3.43) will be zero. Further, for $V < \frac{V_o \chi}{2}$, $\frac{V_o \chi}{2V} > 1$ and, hence, the square brackets in the second term can be removed. Therefore, for S one gets

$$S = 3 \ln \frac{2V}{V_o \chi^{1/3}} \quad . \tag{3.46}$$

Since even for heavy ions like ^{238}U-ion $\chi \approx 8$ the lower limit $V = \frac{V_o \chi^{1/3}}{2} \approx V_o$, Eq. (3.46) will hold for range calculations for any ion. Below $V \approx V_o$, nuclear collisions accompanied by large angle scattering dominate the energy-loss process and hence, as far as range calculation is concerned, the contribution of electronic collision towards energy-loss below $V = V_o$ can be neglected.

$\chi < 1$

In this case both the logarithmic terms become identical and S is given by

$$S = 2 \ln \left(\frac{2V}{V_o} \right)^2$$

$$= 2 \ln \left(\frac{2mV^2}{I} \right) \tag{3.47}$$

3.4 STOPPING POWER EQUATIONS

After substitution of the expressions for S from Eqs. (3.18), (3.26), (3.27), (3.31), (3.33), (3.35), (3.38), (3.40), (3.42), (3.44), (3.45), (3.46) and (3.47) in Eq. (3.1) and conversion to proper units and simplification one obtains the following expressions for the stopping-powers, in MeV-cm^2/mg, valid under the conditions specified.

(i) $X > 1$, $V \gtrsim \frac{Z_2 V_o X}{2}$:

$$\frac{dE}{dX} = \frac{63.65\, z^2}{A_2 V^2}\, Z_2 \log_{10} \frac{11.39\, V^2}{\bar{I} X} \tag{3.48}$$

(ii) $X > 1$, $\frac{Z_2 V_o X^{1/3}}{2} > V > \frac{(Z_2-2) V_o X}{2f(Z_2)}$, $\frac{Z_2 V_o}{2} X > V > \frac{Z_2 V_o X^{1/3}}{2}$:

$$\frac{dE}{dX} = \frac{63.65\, z^2}{A_2 V^2} \{ (Z_2-2) \log_{10} \frac{11.39\, V^2}{\bar{I} X} + 3 \log_{10} \frac{2V}{Z_2 V_o X^{1/3}} \} \tag{3.49}$$

(iii) $X > 1$, $\frac{Z_2 V_o X^{1/3}}{2} > \frac{(Z_2-2) V_o X}{2f(Z_2)}$, $\frac{Z_2 V_o X^{1/3}}{2} > V > \frac{(Z_2-2) V_o X}{2f(Z_2)}$:

$$\frac{dE}{dX} = \frac{63.65\, z^2}{A_2 V^2} \cdot (Z_2-2) \log_{10} \frac{11.39\, V^2}{\bar{I}_1 X} \tag{3.50}$$

(iv) $X > 1$, $\frac{Z_2 V_o X^{1/3}}{2} < \frac{(Z_2-2) V_o X}{2f(Z_2)}$, $\frac{Z_2 V_o X}{2} > V > \frac{(Z_2-2) V_o X}{2f(Z_2)}$:

Eq. (3.50) will also be applicable in this region.

(v) $\chi > 1$, $\frac{Z_2 V_o \chi^{1/3}}{2} < \frac{(Z_2-2) V_o \chi}{2f(Z_2)}$, $\frac{(Z_2-2) V_o \chi}{2f(Z_2)} > V > \frac{Z_2 V_o \chi^{1/3}}{2}$:

$$\frac{dE}{dX} = \frac{13.79\ z^2}{A_2 V^2} \{3(Z_2-2) + 3(Z_2-2) \ln \frac{2f(Z_2) V}{(Z_2-2) V_o} + 6 \ln \frac{2V}{Z_2 V_o} + 2 \frac{f(Z_2) V_o}{V_o \chi} - Z_2 \ln \chi \} \qquad (3.51)$$

(vi) $\chi > 1$, $\frac{Z_2 V_o \chi^{1/3}}{2} < \frac{(Z_2-2) V_o \chi}{2f(Z_2)}$, $\frac{Z_2 V_o \chi^{1/3}}{2} > V > \frac{(Z_2-2) V_o \chi^{1/3}}{2f(Z_2)}$:

$$\frac{dE}{dX} = \frac{13.79\ z^2}{A_2 V^2} \{3(Z_2-2) + \frac{2f(Z_2) V}{V_o \chi} - 3(Z_2-2) \ln \frac{(Z_2-2)(V_o \chi^{1/3}}{2V f(Z_2)} \} \qquad (3.52)$$

(vii) $\chi > 1$, $\frac{Z_2 V_o \chi^{1/3}}{2} > \frac{(Z_2-2) V_o \chi}{2f(Z_2)}$, $\frac{(Z_2-2) V_o \chi}{2f(Z_2)} > V > \frac{(Z_2-2) V_o \chi^{1/3}}{2f(Z_2)}$:

Eq. (3.52) would be also applicable in this region.

(viii) $\chi > 1$, $V < \frac{(Z_2-2) V_o \chi^{1/3}}{2f(Z_2)}$:

$$\frac{dE}{dX} = \frac{12.68\ z^2}{A_2 V} f(Z_2) (3 \chi^{-1/3} + \chi^{-1}) \qquad (3.53)$$

(ix) $\chi < 1$, $V \geqslant \frac{Z_2 V_o}{2}$:

$$\frac{dE}{dX} = \frac{63.65\ z^2 Z_2}{A_2 V^2} \log_{10} \frac{11.39\ V^2}{\bar{I}} \qquad (3.54)$$

(x) $\chi < 1, \quad \frac{Z_2 V_o}{2} > v > \frac{(Z_2-2)V_o}{2f(Z_2)}$:

$$\frac{dE}{dX} = \frac{63.65\, z^2}{A_2 v^2} (Z_2-2) \log_{10} \frac{11.39\, v^2}{\bar{I}_1} \tag{3.55}$$

(xi) $\chi < 1, \quad v < \frac{(Z_2-2)V_o}{2f(Z_2)}$:

$$\frac{dE}{dX} = \frac{50.6}{A_2 v} z^2 f(Z_2) \tag{3.56}$$

The following equations hold in the case of hydrogen as the stopping medium:

(xii) $\chi > 1, \quad v > \frac{V_o \chi}{2}$:

$$\frac{dE}{dX} = \frac{63.65\, z^2}{v^2} \log_{10} \frac{11.39\, v^2}{I \chi} \tag{3.57}$$

(xiii) $\chi > 1, \quad \frac{V_o \chi}{2} > v > \frac{V_o \chi^{1/3}}{2}$:

$$\frac{dE}{dX} = \frac{47.74\, z^2}{v^2} \log_{10} \frac{11.39\, v^2}{I \chi^{2/3}} \tag{3.58}$$

(xiv) $\chi < 1, \quad v > \frac{V_o}{2}$:

$$\frac{dE}{dX} = \frac{63.65\, z^2}{v^2} \log_{10} \frac{11.39\, v^2}{I} \tag{3.59}$$

In all the above equations V and V_o (= 2.185×10^8 cm/sec) are expressed in units of 10^8 cm/sec, and $\bar{I}$, $\bar{I}_1$ and I (= 13.6 eV) in eV. A_2 and Z_2 are the mass and atomic numbers of the stopping medium. z is the ionic charge in units of the electronic charge e. The proper equations for $\bar{I}$, $\bar{I}_1$, $f(Z_2)$ and z are given in next sections (3.5) and (3.6).

3.5 MEAN IONIZATION POTENTIAL

In Bethe's stopping power equation, already mentioned earlier (Section 2.3.2),

$$\frac{dE}{dX} = \frac{4\pi z^2 e^4}{m V^2} Z \ln \frac{2mV^2}{I} \qquad (3.60)$$

I stands for the mean excitation potential of the medium of atomic number Z. This parameter is defined by

$$Z \ln I = \sum_i f_i \ln (\hbar \omega_i) \qquad (3.61)$$

where the summation is extended over the various virtual oscillators of strength f_i and frequency ω_i. These oscillators are attributed to the transition probabilities of the individual atomic electrons. It is quite difficult to obtain accurate estimates of I on purely theoretical grounds.[11] Most workers have to obtain the values of I for a given medium from Bethe's equation with the help of experimental values of the energy-loss of a known ion with known initial velocity. Bloch[9] put forward

the idea that, on the basis of the Thomas-Fermi statistical model, the mean excitation potential should be proportional to the atomic number Z,

$$I = KZ \tag{3.62}$$

where K is a constant. The difficulty, however, was that when the values of I for many media were obtained from Bethe's equation using experimental values of $\frac{dE}{dX}$, the values of K were found to vary with the media. Further, the variation of K with Z is such[8] that it is difficult to make any interpolations or extrapolations on the basis of known values of K to obtain the mean excitation potential for an unknown medium.

Mukherji[12] obtained a relatively simple formula for the calculation of I. He used the assumption, initially made by Bohr,[3] that, as a first approximation, the mean excitation potential I is identical with the mean ionization potential $\bar{I}$.

$$Z \ln I = Z \ln \bar{I} = \sum_{s=1}^{s=Z} \ln I_s , \tag{3.63}$$

where I_s is the mean ionization potential of the s^{th} electron and the summation includes all the Z electrons of the atom of the medium. The summation was replaced by an integration

$$Z \ln \bar{I} = \sum_{s=1}^{s=Z} \ln I_s = \int_{U_s=0}^{U_s=ZV_o} (\ln I_s)\, dn(U_s)$$

$$= \int_{U_s=0}^{U_s=ZV_o} \ln \left(\tfrac{1}{2} m U_s^2\right)\, dn(U_s), \qquad (3.64)$$

where m is the mass of the electron, U_s is the velocity of the s^{th} orbital electron and $n(U_s)$ is the number of electrons having velocity less than a given velocity U_s. For $n(U_s)$ Mukherji and Srivastava[4] have given the following expression mentioned earlier,

$$n(U_s) = f(Z) \frac{U_s}{V_o} \qquad (3.12)$$

where $f(Z) = 0.28\, Z^{2/3}$ for $Z \leqslant 45.5$, (3.65)

$$f(Z) = Z^{1/3} \text{ for } Z > 45.5 . \qquad (3.66)$$

However, Eqs. (3.65) and (3.66) do not hold for either the innermost or the outermost electrons of the atom. After appropriate modification, the expression for $\bar{I}$ was given as[12]

$$Z \ln \bar{I} = (Z-2) \ln \left[13.6 \left\{\frac{Z-2}{2.717\, f(Z)}\right\}^2\right] + 2 \ln (13.6\, Z^2) \qquad (3.67)$$

where $\bar{I}$ is given in eV. The values of $\bar{I}$ predicted by Eq. 3.67) were in fair agreement with the values of I obtained through experiments in the cases of light and heavy elements. There was considerable disagreement in the case of medium-weight

elements of atomic number, $13 < Z < 74$. Significantly, the calculated ranges of heavy ions in nickel and silver as stopping media show large deviation from the experimental values.[13] Since all stopping-power equations contain $f(Z)$ directly or through $\bar{I}$ and $\bar{I}_1$, it was assumed that a new prescription is needed for the calculation of $f(Z)$. There are three reasons for the assumption. Firstly, there is a large difference between the experimental values of the mean ionization potentials and those calculated using Mukherji's[12] equation in the case of elements of atomic number Z in the region $74 > Z > 26$. Secondly, from the theoretical point of view Eqs. (3.65) and (3.66) were obtained from a consideration of the interaction between a moving ion and only a few outer orbital electrons, except in the case of very light media, and, hence, should be valid only for the outermost electrons, whereas their use in Eq. (3.67) implies their validity for all orbital electrons except the two K-shell electrons. Lastly, since $f(Z)$ largely represents the "effective quantum number" of the electrons, which, as Bohr[3] argued would be unity for the outermost and the innermost orbital electrons, the values given by Eqs. (3.65) and (3.66) for $f(Z)$ are possibly overestimations for medium-weight and heavy-weight elements, particularly at high ion energies when a majority of orbital electrons are involved in the interaction. Thus, one should take values of $f(Z)$ averaged over all orbital electrons; these would be smaller than the values obtained using Eqs. (3.65) and (3.66), would lead to larger values of $\bar{I}$, and would, therefore, be consistent with

the experimental values.[13] To obtain the new expression for f(Z) Eq. (3.67) was assumed to be basically valid and that by substituting the experimental values of the mean excitation potentials in place of $\bar{I}$ in that equation one would obtain the averaged or new values of f(Z). The experimental values taken from Bakker and Segrè,[14] as calculated by Bethe and Ashkin[11] and from the compilation of Barkas and Berger[15] are shown in Table 3.1. Figure 3.1 shows a logarithmic plot of the new f(Z) values against log Z. A least squares fit yields the relation

$$f(Z) = 0.3634\ Z^{0.555} \tag{3.68}$$

which on substitution in Eq. (3.67), gives

$$Z \ln \bar{I} = (Z-2) \ln \{ \frac{13.95\ (Z-2)^2}{Z^{1.10}} \} + 2 \ln (13.6\ Z^2) \tag{3.69}$$

and

$$\bar{I}_1 = \frac{13.95\ (Z-2)^2}{Z^{1.10}} \quad . \tag{3.70}$$

For $Z < 13$ and $Z > 74$, the values of f(Z) from Eq. (3.68) differ very little from those obtained by the earlier equations Eqs. (3.65) and (3.66), but for $13 < Z < 74$, there is a 13-17% lowering in the values of f(Z). Table 3.2 lists the newly calculated values of $\bar{I}$ for some elements along with the corresponding accurate experimental values from Andersen *et al.*[16] and Sørensen and Andersen[17] which have not been used as inputs in obtaining the relation given by Eq. (3.68). Since the earlier expressions

Table 3.1

The experimental mean excitation potentials (in eV) used in obtaining the expression $f(Z) = 0.3634\ Z^{0.555}$

Element	Atomic number, Z	I^a	I^b
Li	3	34	38
Be	4	60.4	60
C	6	76.4	78
N	7		85
O	8		89
Ne	10		131
Al	13		163
Ar	18		210
Fe	26	241	285
Cu	29	276	314
Ag	47	418	487
Sn	50	463	516
W	74	655	748
Au	79		797
Pb	82	705	826
U	92	811	

[a] Bakker and Segrè (ref. 14).

[b] Barkas and Berger (ref. 15).

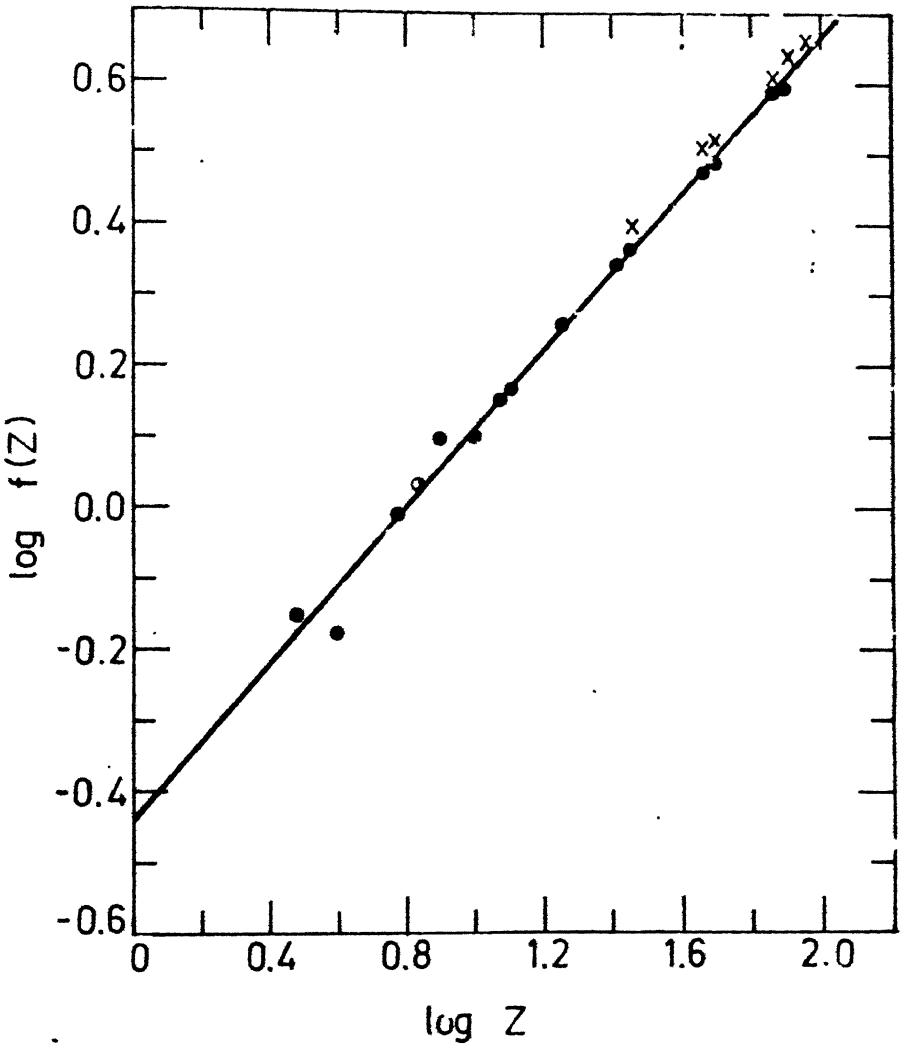

Fig.3.1 Plot of $\log_{10} f(Z)$ versus $\log_{10} Z$. x and • are based on the data from Bakker and Segre' (Ref. 14) and Barkas Berger .(Ref. 15) respectively.

Table 3.2

Comparison between the calculated values of $\bar{I}$ with the experimental values of mean excitation potential I

Element	Atomic number, Z	I (eV) Experimental	$\bar{I}$ (eV) Calculated
Ca	20	195.0[a]	231.2
Sc	21	217.0[a]	241.0
Ti	22	229.0[a]	250.7
V	23	238.7[a]	260.2
Cr	24	259.1[a]	269.8
Mn	25	273.8[a]	279.2
Fe	26	280.8[a]	288.6
Co	27	299.3[a]	297.9
Ni	28	303.4[a]	307.1
Cu	29	321.7[a]	316.3
Zn	30	323.4[c]	325.4
Ag	47	466.8[b]	474.0
Au	79	750.0[b]	733.8
Pb	82	766.0[b]	757.4
U	92	831.0[b]	835.0

[a] H.H. Andersen, H. Sørensen and P. Vajda (ref. 16).

[b] H. Sørensen and H.H. Andersen (ref. 17).

for f(Z) were deduced from the ranges of fission products, the new f(Z) values from Eq. (3.68) would yield considerably larger values for calculated fission product ranges. As fission products are essentially heavy ions having low initial kinetic energies in the range 0.5 - 1.0 MeV/amu, in all stopping power calculations Eq. (3.68) has been used at ion energies greater than 1.0 MeV/amu while below that energy Eqs. (3.65) and (3.66) have been used.

3.6 CALCULATION OF THE ION CHARGE

At low ion velocities, comparable to those of outer atomic electrons, capture and loss of electrons by the penetrating ion complicates the energy-loss calculations. With increasing atomic number of the ion, over wide ion-velocity region, charge fluctuations become important. However, the processes involved in capture and loss of electrons by a moving ion are in general so intricate as to defy any precise and comprehensive formulation.

According to Bohr,[3] an ion penetrating a material medium loses all electrons whose orbital velocities, U_s, are less than the ion velocity V. Therefore, the charge number of the ion (z) will be the same as $n(U_s)$ with $U_s=V$ in Eq. (3.12)

$$z = n(U_s=V) = f(Z_1) \frac{V}{V_o} \tag{3.71}$$

where Z_1 is the atomic number of the ion and $f(Z_1)$ is given by Eq. (3.68) with $Z= Z_1$. Equation (3.71) has been found to hold

good only for ions which are less than half stripped, that is, $z < \frac{Z_1}{2}$.[4,18] For higher ion velocities at which the ion is more than half stripped, Srivastava and Mukherji[5] have given the following expression for calculating the ion charge,

$$z = Z_1\{1 - c \exp(-2f(Z_1)V/Z_1V_o)\} . \qquad (3.72)$$

Since the ion charge can be predicted quite well using Eq.(3.71) for ion velocities $V \leqslant \frac{Z_1V_o}{2f(Z)}$, that is when $z \leqslant \frac{Z_1}{2}$, the constant c in Eq. (3.72) can be obtained by assuming that at $V = \frac{Z_1V_o}{2f(Z)}$, Eq. (3.71) makes a smooth transition to Eq. (3.72):

$$z = Z_1 \{1 - 2.039 \exp(-2V f(Z_1)/Z_1V_o)\}. \qquad (3.73)$$

Though semi-empirical in nature, the good agreement between the calculated and the experimental values justifies the use of Eqs. (3.71) and (3.73) from the point of view of practical utility.

3.7 RANGE COMPUTATIONS

The energy transferred to the atomic electrons of the stopping medium in a single collision by a fast moving heavy ion is quite large compared to chemical bond energies. Therefore, the fast moving ion does not essentially see any chemical bond between the atoms of the compound. Hence, the stopping power of the compound medium can be calculated by summing up the stopping

powers of the component elements taking into account the partial density of each elemental component as follows. The stopping power $\left[\left(\frac{dE}{dX}\right)_i\right]_E$ of the i^{th} atomic species in its pure elemental state at a particular ion-energy E is given by

$$\left[\left(\frac{dE}{dX}\right)_i\right]_E = \frac{2\pi z^2 e^4}{mV^2} \; n_i \, S_i \qquad (3.74)$$

where n_i is the number of atoms per unit volume and S_i is defined by Eq. (3.10). Eq. (3.74) can also be written as

$$\left[\left(\frac{dE}{dX}\right)_i\right]_E = \frac{2\pi z^2 e^4}{mV^2} \; \frac{\rho_i N}{A_i} S_i \;, \quad \text{or}$$

$$\left[\frac{1}{\rho_i}\left(\frac{dE}{dX}\right)_i\right]_E = \frac{2\pi z^2 e^4}{mV^2} \; \frac{N}{A_i} \; S_i \qquad (3.75)$$

where ρ_i is the density of the pure i^{th} atomic species of atomic mass A_i, and N is the Avogadro number. For the complex medium the stopping-power $\left[\left(\frac{dE}{dX}\right)_i\right]_E$ at ion energy E is given by

$$\left[\left(\frac{dE}{dX}\right)_c\right]_E = \frac{2\pi z^2 e^4}{mV^2} \; n_c \sum_i Y_i \, S_i \qquad (3.76)$$

where n_c is the number of molecules of the compound per unit volume, and Y_i is the number of atoms of the i^{th} atomic species per molecule. If A_c is the molecular mass and ρ_c is the density of the complex medium, Eq. (3.76) can be rewritten as

$$\left[\left(\frac{dE}{dX}\right)_c\right]_E = \frac{2\pi z^2 e^4}{mV^2} \frac{\rho_c N}{A_c} \sum_i Y_i S_i$$

or, $$\left[\left(\frac{1}{\rho_c}\frac{dE}{dX}\right)_c\right]_E = \frac{1}{A_c} \sum_i A_i Y_i \left[\left(\frac{1}{\rho_i}\frac{dE}{dX}\right)_i\right]_E , \qquad (3.77)$$

after substituting for S_i from Eq. (3.74). The range R of the ion can be computed numerically:

$$R = \sum_{E_i}^{E_o} \frac{\delta E}{\left[(dE/dX)_c\right]_E} ; \qquad (3.78)$$

the energy interval δE should be sufficiently small ($\sim$0.01 MeV) so that the stopping power remains sensibly constant over this small interval; E_i is the initial energy of the ion and E_o is the energy corresponding to ion-velocity V_o. After the ion has slowed down to the velocity V_o its energy loss occurs largely through nuclear collisions. These involve random large-angle scatterings, the net result of which is that the ion does not penetrate much in it's original direction after the velocity becomes less than V_o. The numerical computations were done using an IBM 7044 computer. The computer was provided with the equations (Eqs. (3.48) - (3.59)) for stopping powers, Eqs. (3.71) and (3.73) for calculating the ionic charges, along with the velocity regions in which they are valid. $\bar{I}$ and $\bar{I}_1$ were calculated using Eqs. (3.69) and (3.70 respectively. The f(Z) values in all the above equations were obtained by mean of Eq. (3.68).

The energy of the ion was changed in steps of $\delta E = 0.01$ MeV from the initial energy E_i (= 10 MeV/amu) to the lower limit E_o corresponding to the velocity V_o. The stopping powers were obtained using appropriate equations for each energy interval and the ranges were calculated using Eq. (3.78). Ranges were also calculated with $\delta E = 0.001$ MeV in a few cases. The ranges so obtained, however, differed from those calculated with $\delta E =$ 0.01 MeV by < 1%.

3.8 RESULTS AND DISCUSSION

3.8.1 Ranges in Elemental Media

Since many of the stopping power equations presented here differ from those obtained by Srivastava and Mukherji,[5] it was necessary to check the validity of these equations for simple elemental media before using them in the case of complex media. The energy-losses for ^{19}F, ^{16}O, ^{14}N, ^{12}C, ^{11}B and ^{10}B ions with initial energies of 10 MeV/amu in passing through various thickness of oxygen gas were calculated using the procedure described in the earlier section. The calculated energy-loss curves are compared with the experimental values from Roll and Steigert[19] in Figs. 3.2 and 3.3. In Fig. 3.4 the calculated energy-loss curves for ^{40}Ar and ^{12}C ions in nitrogen and argon gas are compared with the corresponding experimental values from Martin and Northcliffe.[20] Nitrogen, oxygen and argon are typical light media and, as the Figs. 3.2, 3.3 and 3.4 show, the agreement

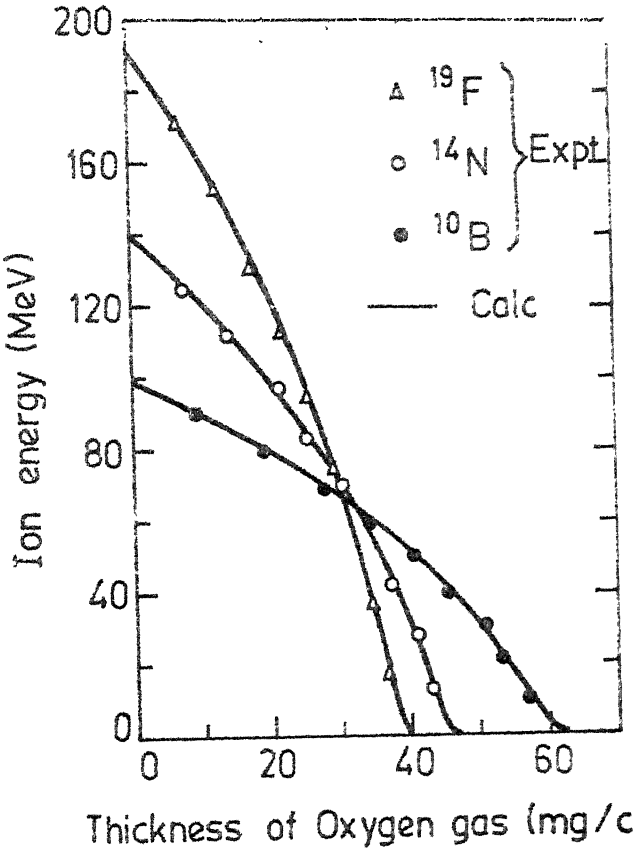

Fig. 3.2 Energy-loss curves for ^{19}F, ^{14}N and ^{10}B ions in Oxygen gas. Experimental data are from Roll and Steigert (Ref. 19)

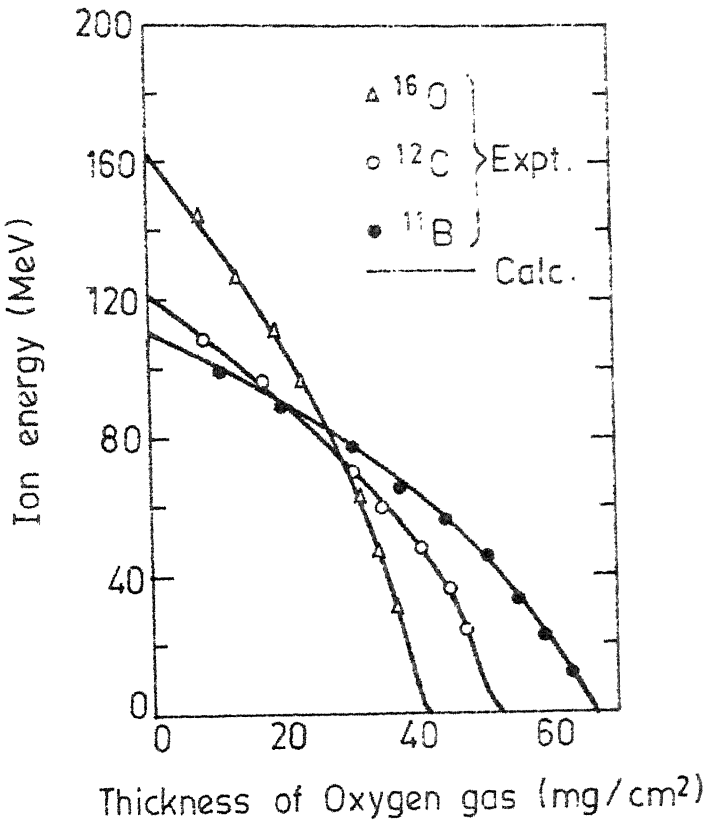

Fig. 3.3 Energy-loss curves for ^{16}O, ^{12}C and ^{11}B ions in Oxygen gas. The experimental data are fron Roll and Steigert (Ref. 19)

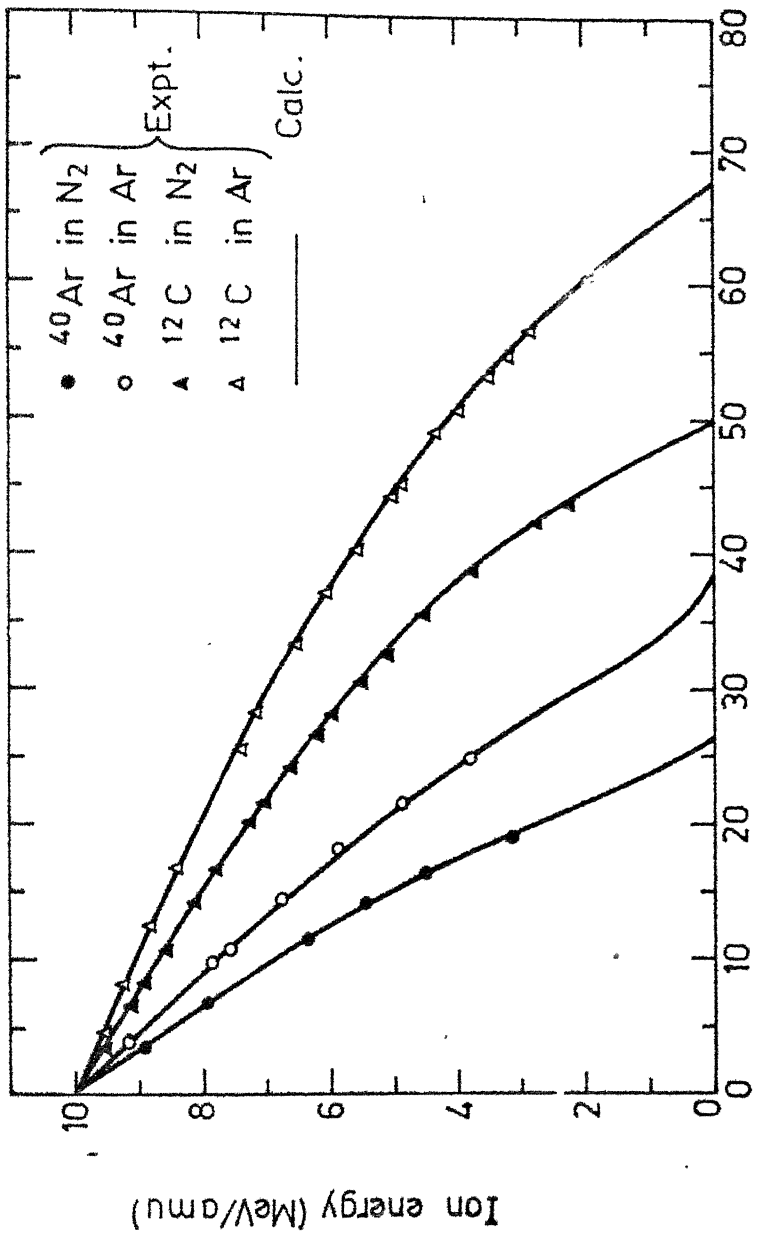

Fig. 3.4 Energy-loss curves for ^{12}C and ^{40}Ar ions in gaseous Nitrogen and Argon. The experimental data are from Martin and Northcliffe (Ref.20)

between the calculated and the experimental values is quite good. For light stopping media, however, even the earlier calculations[5] were in good agreement with the experimental values. It was in the case of heavy stopping media like nickel that the earlier results[5] were in considerable disagreement with the experimental values. Hence, it is crucial to ascertain the applicability of the present stopping power equations to heavy stopping media. In Figs. 3.5, 3.6 and 3.7 the calculated energy loss curves for ^{10}B, ^{11}B, ^{12}C, ^{14}N, ^{16}O, ^{19}F and ^{20}Ne-ions in nickel are compared with the experimental data from Roll and Steigert.[19] The calculated energy-loss curves for ^{12}C-ions in silver using both the old and new f(Z) values are shown in Figure 3.8 along with the experimental values from Walton and Hubbard.[21] The good agreement between the calculated and experimental values for nickel and silver shows that the present stopping power equations can be used for medium-weight elements as stopping media.

3.8.2 Compound Media

Schambra et al.[22] have measured the energy-loss suffered by accelerated heavy ions of initial energies of 10 MeV/amu in passing through different thicknesses of mylar ($C_{10}H_8O_4$) and polyethylene, $(CH_2)_n$. The energies of the incident and the emergent ion were measured with magnetic spectrograph. The experimental energy-loss curves for ^{12}C, ^{16}O-ions in polyethylene, and ^{12}C, ^{16}O, ^{20}Ne-ions in mylar are compared with the calculated ones in Figs. 3.9 and 3.10 respectively. For calculating the

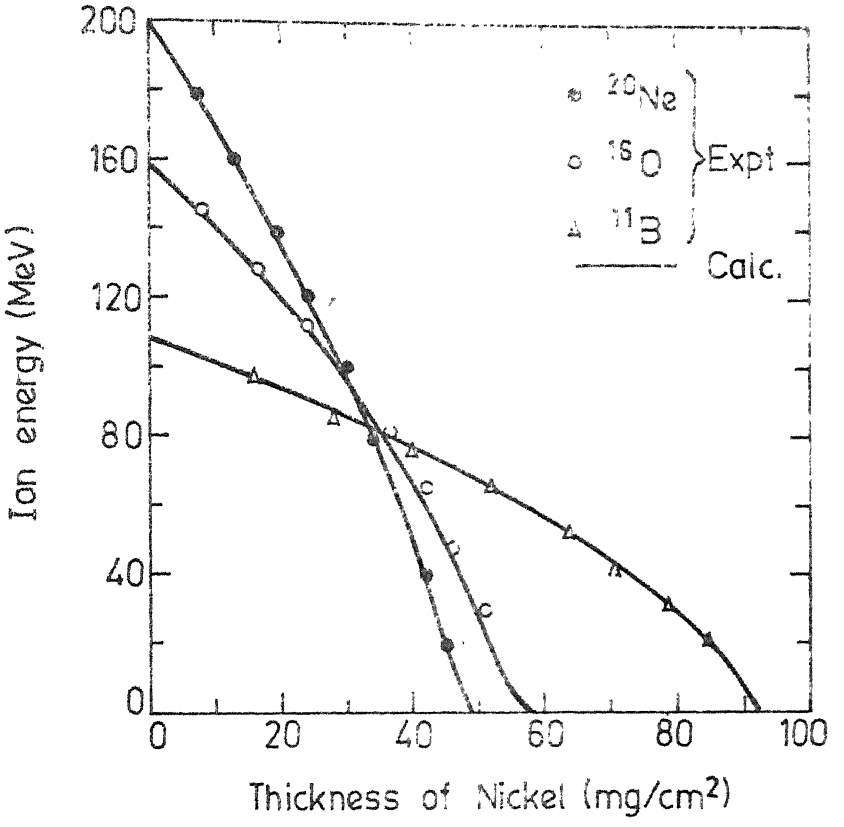

Fig. 3.5 Energy-loss curves for ^{20}Ne, ^{16}O and ^{11}B ions in Nickel. The experimental data are from Roll and Steigert (Ref. 19)

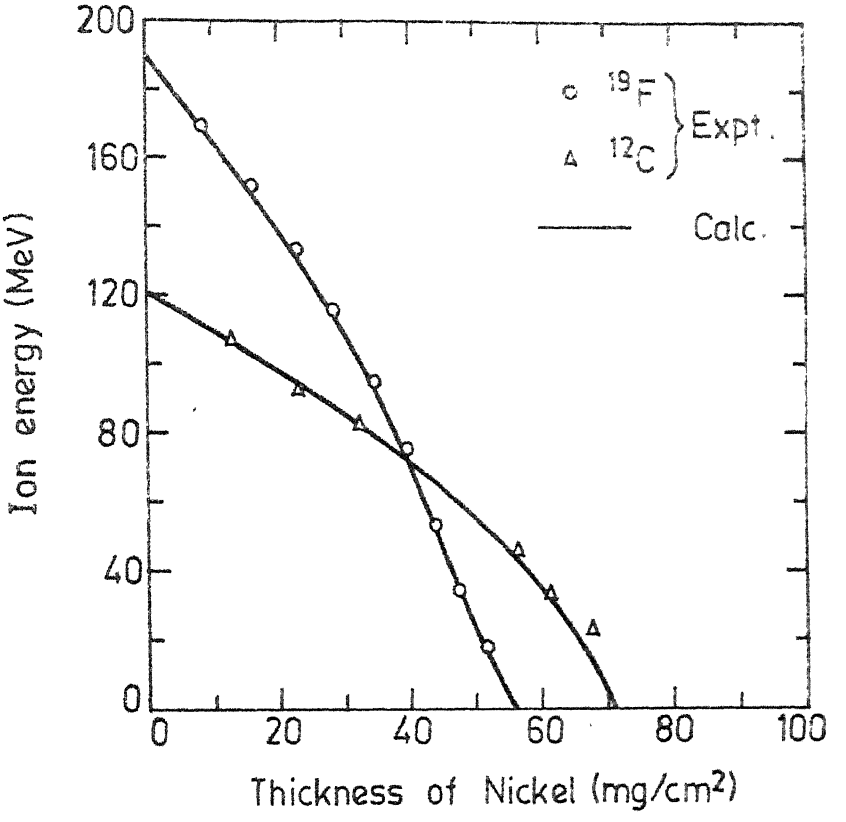

Fig. 3.6 Energy-loss curves for ^{19}F and ^{12}C ions in Nickel. The experimental data are from Roll and Steigert (Ref. 19)

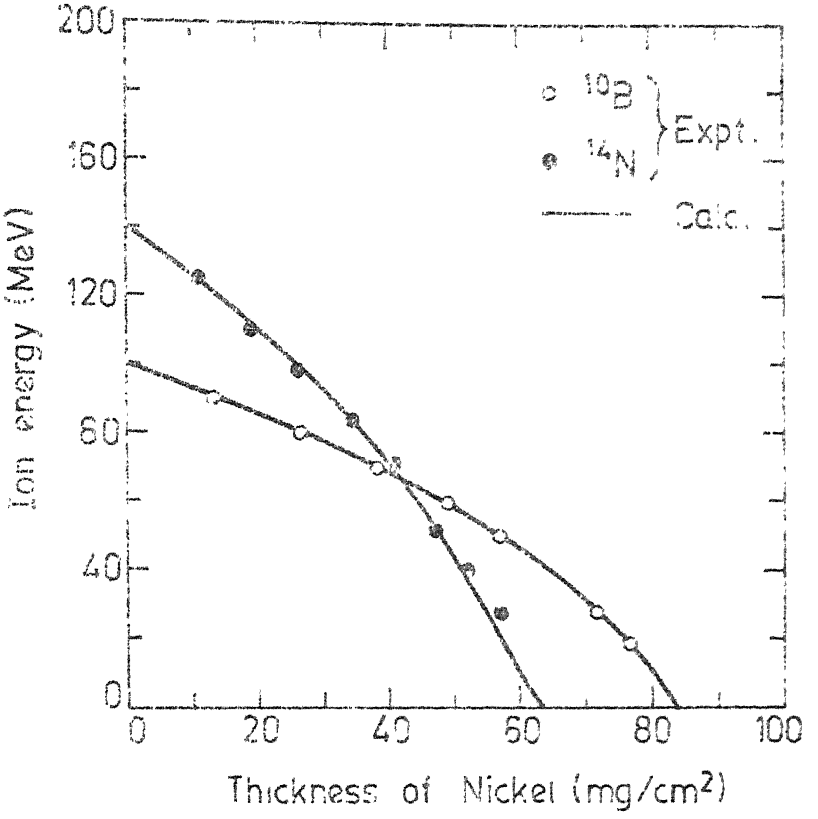

Fig. 3.7 Energy-loss curves for ^{10}B and ^{14}N ions in Nickel. The experimental data are from Roll and Steigert (Ref. 19)

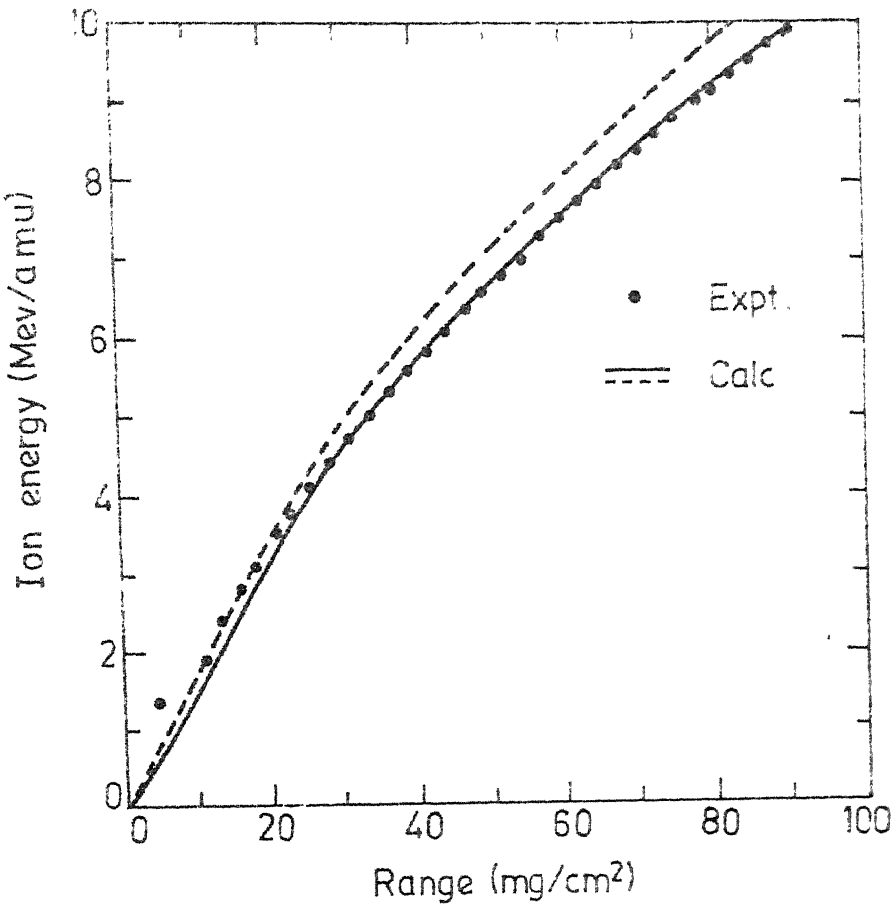

Fig. 3.8 Range-energy curve for ^{12}C ions in silver. The experimental data are from Walton and Hubbard (Ref. 21). The solid and dashed lines represents the ranges calculated using the new and old f(z) values respectively.

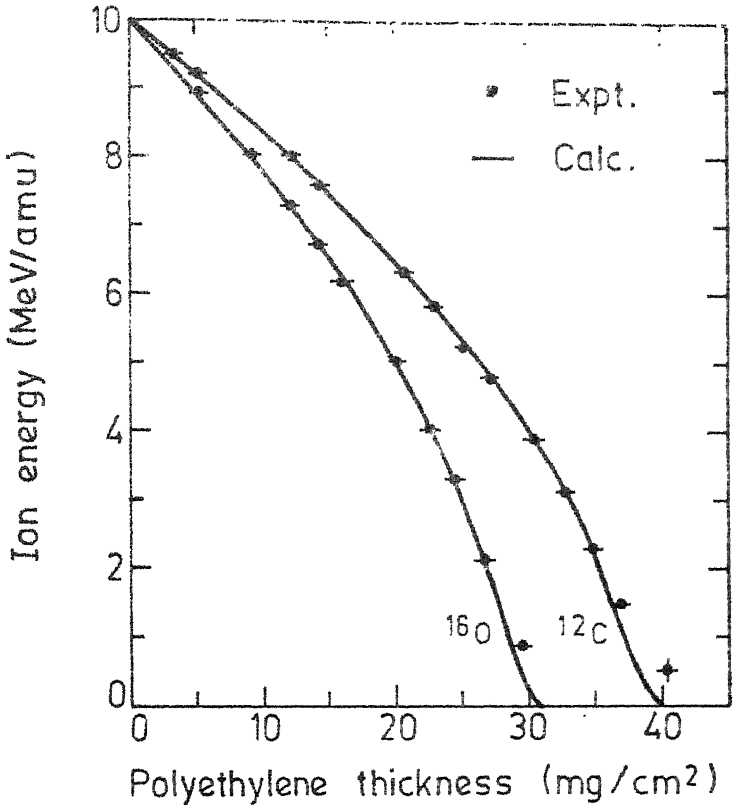

Fig. 3.9 Energy-loss curves for ^{12}C and ^{16}O ions in polyethylene. The experimental data are from Schambra etal (Ref. 22)

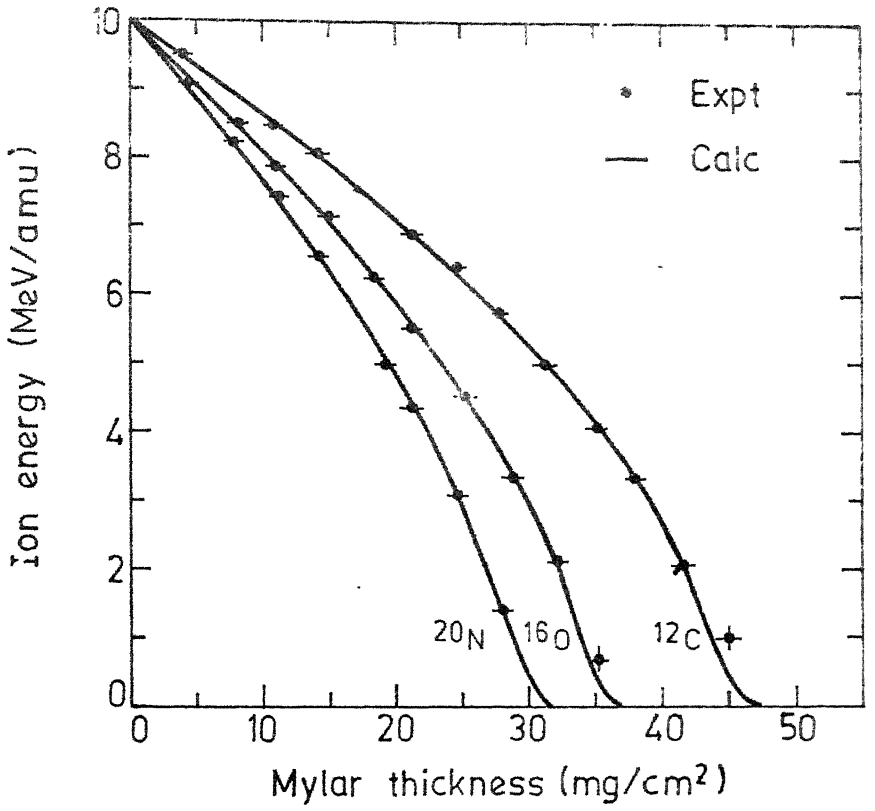

Fig. 3.10 Energy-loss curves for ^{12}C, ^{16}O and ^{20}Ne ions in Mylar. The experimental data are from Schambra etal (Ref. 22)

energy-loss, the compound media was treated as a homogeneous mixture of the constituent elements and chemical binding was neglected. Energy-loss curves have also been calculated for simulated tissue material having the chemical composition $C_7H_{70}N_2O_{32}$[23] for the ions ^{11}B, ^{12}C, ^{16}O and ^{20}Ne and compared with the corresponding experimental values from Brustad[24] in Fig. 3.11. In all the cases the agreement between the calculated and the experimental values appears to be good. Mylar, and polyethylene and the simulated tissue material, however, contain only light elements and the present results are not significantly different from those obtained by Srivastava and Mukherji[5] for these particular media.

3.8.3 Nuclear Research Emulsions

Nuclear research emulsions contain finely divided (micron sized) grains of silver bromide uniformly dispersed in gelatin.[25] Since the energy-loss suffered by an ion in passing through a single silver bromide grain can be quite large, the nuclear emulsions possibly can not be regarded strictly as homogeneous media at molecular level. Ranges in G-5 nuclear emulsion were calculated by using two different procedures. In the first procedure the nuclear emulsion was considered as a homogeneous medium while in the second procedure the heavy ion was considered as passing alternately through segments of silver bromide grains and gelatin each retaining its own bulk density.

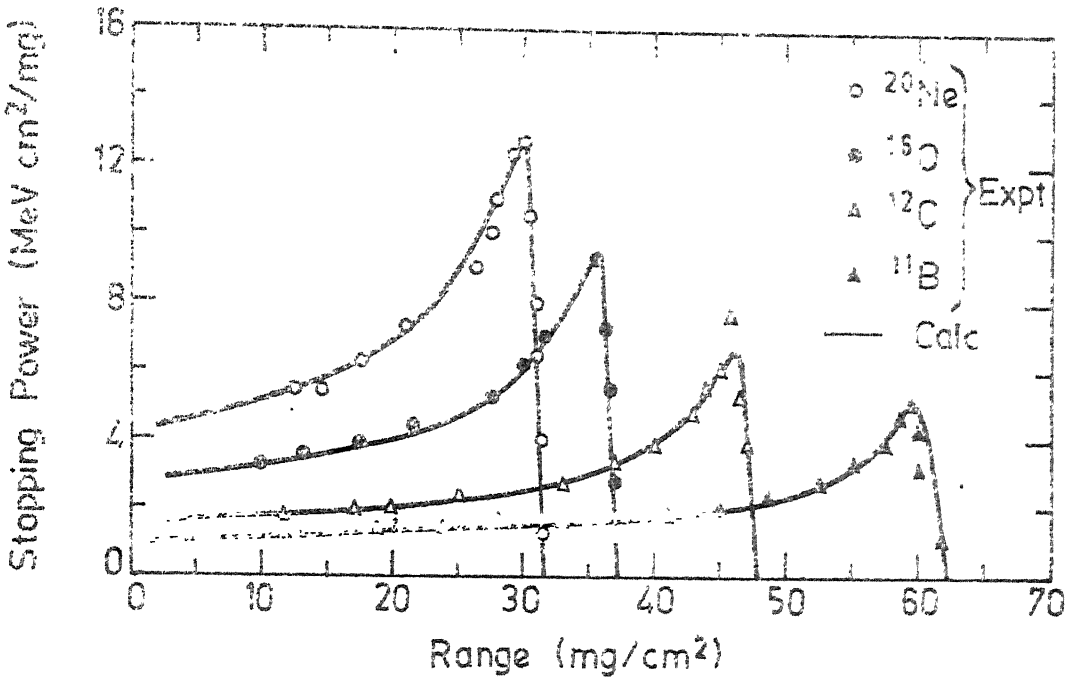

Fig. 3.11 Plots of stopping power of ^{11}B, ^{12}C, ^{16}O and ^{20}Ne ions against their penetration depth in tissue material. The experimental data are from Brustad (Ref. 24)

From the composition of the "standard" G-5 nuclear emulsion,[25] given in percentage by weight, one obtains the following empirical formula (Appendix) for G-5 nuclear emulsion of density 3.815 g/cm^3:

$$AgBr_{0.994}I_{0.006}C_{1.370}N_{0.314}S_{0.013}H_{3.185}O_{0.932}$$

when the emulsion is under vacuum during bombardment, due to the evaporation of water, the density changes to 4.0 g/cm^3. Let $x g/cm^3$ be the weight of water lost when kept under vacuum. Since each gram of water removed causes a reduction in volume of 0.73 cm^3, as obtained from the dehumidification curves,[25] one obtains

$$\frac{3.815 - x}{1 - 0.73x} = 4.0 \qquad (3.79)$$

and hence x = 0.0962. Taking into account the evaporation of water, the new empirical formula is

$$AgBr_{0.995}I_{0.006}C_{1.370}N_{0.314}S_{0.013}H_{2.545}O_{0.626}$$

Assuming the empirical formula of gelatin to be $C_{1.370}N_{0.314}S_{0.013}H_{2.545}O_{0.626}$, and neglecting the small atomic proportion of iodine, the path lengths through gelatin and silver bromide were obtained following the procedure of Barkas.[25] The average grain diameter $\langle D \rangle$ of silver bromide in G-5 nuclear

emulsion[25] is 0.275 μm, with a standard deviation σ= 0.0022 μm. Assuming random traversal of grains the average path length $\langle \delta_s \rangle$ through silver bromide is given by[25]

$$\langle \delta_s \rangle = \frac{2}{3} \langle D \rangle = 0.1833\,\mu m. \qquad (3.80)$$

If n be the number of grains the ion passes through when it traverses unit distance, the average distance ℓ between the centres of two successive silver bromide grains is given by

$$\ell = 1/n \ . \qquad (3.81)$$

The value of n has been calculated from the relation[25]

$$n = \frac{3}{2} \frac{C}{\langle D \rangle} \{(1 + \frac{\sigma^2}{\langle D \rangle^2})(1 - \frac{3\sigma^2}{\langle D \rangle^2}) \} \ , \qquad (3.82$$

where C is the fraction of the volume occupied by silver bromide. In calculating C the change in volume due to evaporation of water during bombardment under vacuum has to be taken into account. The weight of water lost per cm^3 of the original emulsion is 0.0962g, and the corresponding decrease in volume obtained from dehumidification curve is 0.0702 cm^3. Therefore 1 cm^3 of the original emulsion will occupy a volume of 0.9298 cm^3 during bombardment. Thus, if the change in density of the emulsion under vacuum is attributed to the evaporation of water only, 0.9298 cm^3 of the emulsion will contain 3.1407 g of silver bromide.

Assuming that silver bromide retains its bulk density of 6.473 g/cm^3 during bombardment, for C one obtains a vlue of 0.5239. Hence, l is equal to 0.3712 μm and the average path length through gelatin, δ_g, is given by

$$\langle \delta_g \rangle = l - \langle \delta_s \rangle = (0.3721 - 0.1833)\,\mu m$$
$$= 0.1888\,\mu m. \qquad (3.83)$$

The heavy ion passes alternately through an average distance of 0.1888 μm of gelatin and 0.1833 μm of silver bromide.

For computational purpose each silver bromide and gelatin segment was theoretically subdivided into several sections so that the energy-loss suffered by the ion in passing through each section did not exceed 0.01 MeV. The range was obtained by noting the number of segments of silver bromide and gelatin through which the ion passes before its velocity is reduced to V_o. The ranges calculated using this procedure for the ions ^{10}B, ^{11}B, ^{12}C, ^{14}N, ^{16}O, ^{19}F and ^{20}Ne are shown in Figs. 3.12, 3.13 and 3.14 along-with the corresponding experimental values from Roll and Steigert.[26] These calculated ranges did not differ sensibly from those calculated by the first procedure stated earlier. The calculated ranges are systematically larger than the experimental values by $\sim 3\,\mu$m at ion energies below ~ 4.5 MeV/amu for all ions other than ^{20}Ne for which there is almost a constant difference of $\sim 5\,\mu$m at all energies. The small disagreement at low energies can be due to : (i) the distortion of gelatin during the

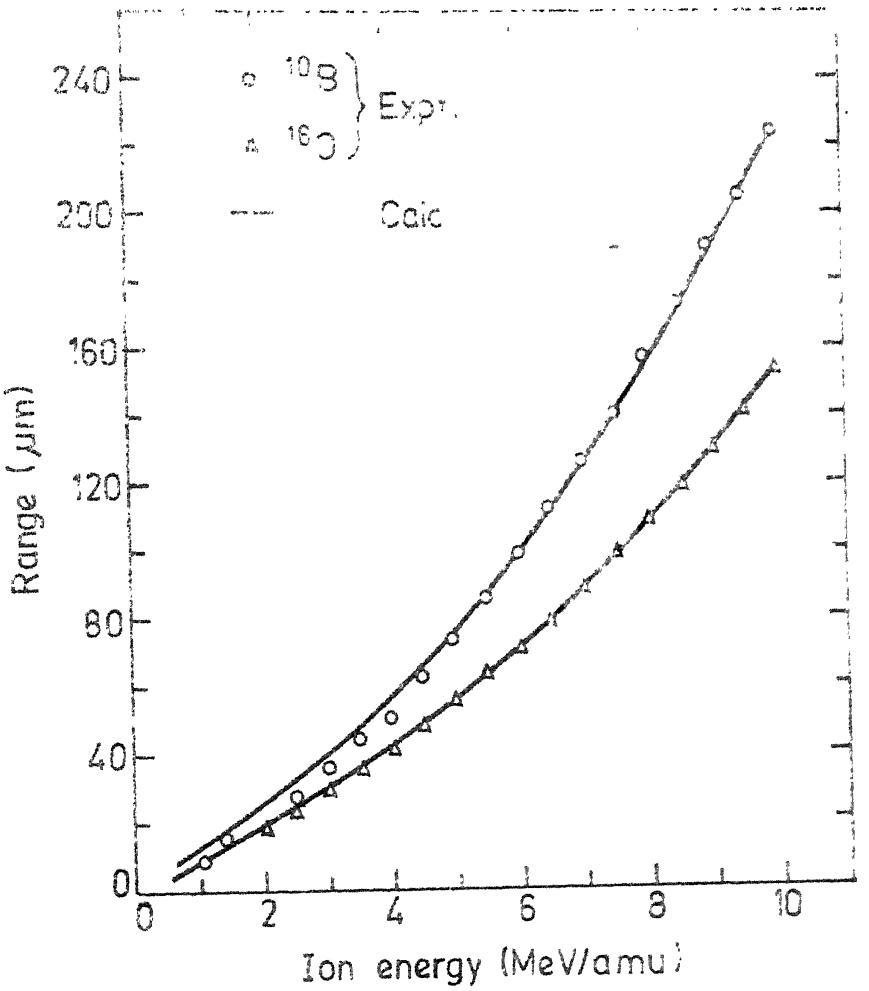

Fig. 3.12 Range-energy curves for ^{10}B and ^{16}O ions in G-5 nuclear emulsion. The experimental data are from Roll and Steigert (Ref. 26)

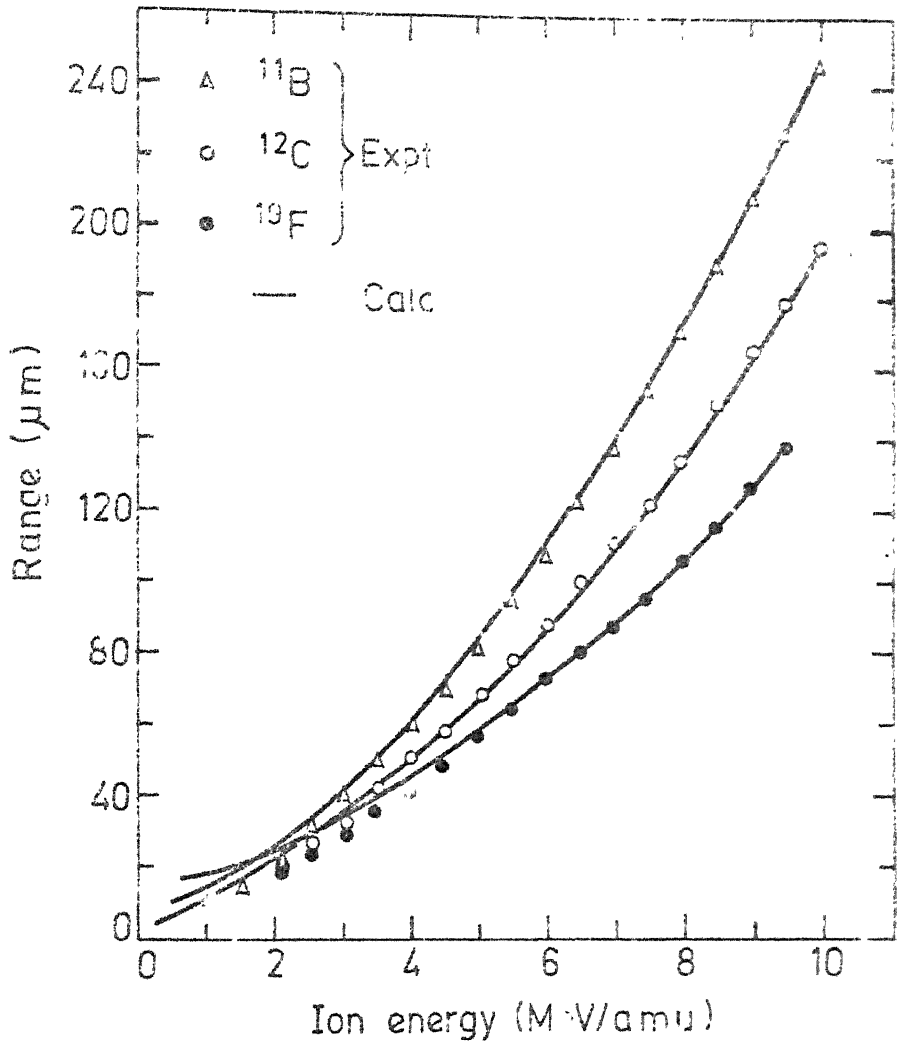

Fig. 3.13 Range-energy curves for ^{11}B, ^{12}C and ^{19}F ions in G-5 nuclear emulsion. The experimental data are from Roll and Steigert (Ref. 26)

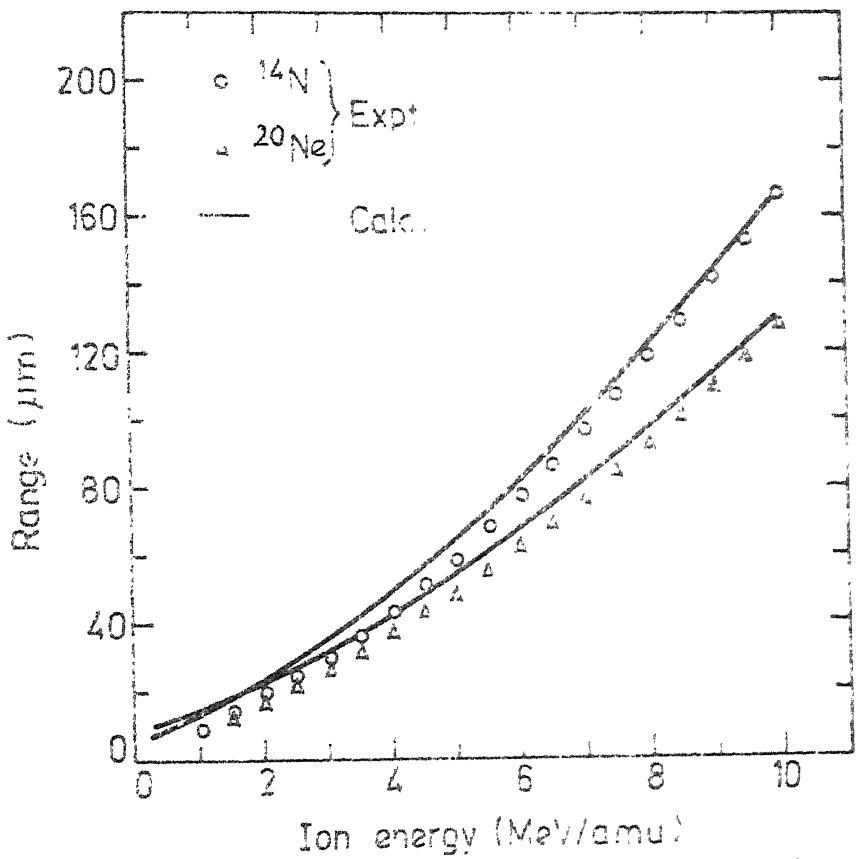

Fig. 3.14 Range-energy curves for ^{14}N and ^{20}Ne ions in G-5 nuclear emulsion. The experimental data are from Roll and Steigert (Ref. 25).

development process involving humidification and heating which can introduce some error in the measured track lengths, particularly for low energy ions, (ii) for heavy ions the uncertainty in their charge state, and, hence, in their kinetic energy, increases as the ion energy decreases below ~4 MeV/amu.[26]

The overall agreement between the calculated and the experimental energy-loss curves appears to be good for all kinds of stopping media, and hence, one can conclude that these stopping power equations along with the modified formula for ionization potential are of general applicability.

CHAPTER 4

TECHNIQUES OF RANGE MEASUREMENTS

4.1 RANGE CONCEPTS

A swiftly moving charged particle loses kinetic energy by various types of interactions which have been discussed earlier, and comes to a halt after penetrating a certain distance of the stopping medium. The penetration depth is called the range. However, since the stopping processes are statistical in nature, there is no unique range for a large number of particles having the same initial kinetic energy and the same initial direction of penetration. Hence, it is customary to define ranges in terms of the "average" range, the "most probable" range and the "median" range. The most probable range is given by the peak in the range distribution curve, and the median range corresponds to the penetration depth beyond which 50% of the incident particles penetrate. If the range distribution curve is gaussian, then all these ranges will have the same magnitude.

It should be noted that experiments give the projection of the actual path in the initial direction of penetration. Only for those cases where slowing down of the energetic particle takes place via a large number of small-angle scattering events does the range and the actual path length have almost the same magnitude. For heavy charged particles having high kinetic energies, the energy-loss is predominantly due to inelastic collisions with the electrons of the stopping medium and the above approximation holds good. However, low energy charged particles in penetrating heavy stopping media lose kinetic energy by collision with atoms of the stopping medium which is accompanied by large-angle scattering and, hence, for these ions there is a considerable difference between the actual path length and the range; since theoretical calculations refer to the total path length, the experimentally obtained ranges may require corrections before any valid comparisons can be made between the two.

4.2 RECOIL TECHNIQUES

When the target nuclei, e.g., ^{235}U, undergo fission, the fraction of a particular fission product escaping from the target depends upon the direction of emission, its range, as well as the thickness of the target. Depending upon whether the target thickness is negligibly small or very large compared to the range of the fission product of interest (also called recoil product), the different experimental methods for range measurement can be

roughly divided into two categories, namely, thin target methods and thick target methods, respectively.[7]

4.2.1 Thin Target Methods

In this method the target has a thickness much less than the range of the recoil product of interest and hence the emerging recoils can be assumed to preserve the original range distribution and the angular distribution.

(i) Thin target-thin catcher differential method- A well-collimated beam of recoil products emerging from a very thin target is allowed to penetrate the catcher material at a known angle of incidence. The catcher can be a stack of thin foils or it can be a thick foil from which layers of uniform thickness can be removed. When a stack of foils is used the thickness of each foil should be small compared to the range of the recoil product to get good differential range curves. The concentration of the recoils in each layer or foil is determined suitably and, from a plot of concentration per layer versus the thickness penetrated, the range of the recoils can be obtained.

The possible sources of error lie in the finite thickness of the target, the finite size of the collimator holes and the non-uniformity in the thickness of the foils used or in the thickness of layers removed from the thick catcher.

(ii) Thin target-thin catcher integral method- A thin target

(source) which is emitting recoils isotropically (like a fissile (source) is kept close to a stack of catcher foils. The activity A_t present beyond a thickness t, from the catcher surface facing the source is related to the range R, is given by Segré and Wiegand,[27] by the equation

$$A_t = k\ (R-t) \quad ,$$

where k is a constant. A plot of A_t versus t gives a straight line and the intercept on the t-axis gives a range R. Finkle et al.[28] used this method for determining the ranges of ^{140}Ba from ^{235}U fission in aluminium catcher.

The sources of error in this method are the finite thickness of the target (source) and the non-uniformity in the thickness of the catcher foils.

4.2.2 Thick Target Methods

One of the main disadvantages of the thin target method is that they are useful only if the target material has a large nuclear reaction cross-section. If the target material has a low reaction-cross section, long periods of irradiation will be required. This difficulty can be overcome by using the thick-target method developed by Sugarman et al.[29]

(i) Thick target-thick catcher method- A target (source), whose thickness is much larger than the range of the recoil product in

it, is sandwiched between two catcher foils. The catcher foils should be thick enough to stop all the recoils of interest. If the recoils are assumed to be emitted isotropically, a reasonable assumption if the target is amorphous and the projectiles are incident on it isotropically, the range R, of the recoil product in the target material is given by

$$R = 4 \frac{A_C}{A_T} t ,$$

where A_C is the activity of the recoil in one of the catchers, A_T is the total activity of the recoil product both in the target and the catcher foils, and t is the thickness of the target. Niday[30] has used this method for measuring the ranges of fission products from the thermal neutron induced fission of ^{235}U.

(ii) Thick target-thin catcher method- Alexander and Gazdik[31] used targets that were not of negligible thickness but were able to obtain ranges of fission products in the catcher material. The target is sandwiched between stacks of catcher foils of different thickness. The fraction F_t of the total yield of a particular kind of recoil product penetrating beyond a given thickness t of the external catcher is given by[31]

$$F_t = \frac{1}{2} \left(1 - \frac{t}{\bar{R}} - \frac{cW}{2\bar{R}}\right)$$

where W is the target thickness and $\frac{1}{\bar{R}}$ is the average reciprocal

range in the catcher material. c is a constant which relates the rate of velocity loss in the target material to the rate of velocity loss in the catcher material, and is given by the equation:

$$\frac{\partial F_t}{\partial W} = - \frac{c}{\bar{4R}} \quad .$$

This method assumes that the recoil products are emitted isotropically.

4.3 NUCLEAR EMULSIONS

Nuclear emulsions contain[32] finely divided grains of silver bromide dispersed uniformly in gelatin. They differ from ordinary photographic emulsions in the following important aspects:

i) Nuclear emulsions contain a high concentration of silver bromide, as much as four times that in ordinary photographic emulsions.

ii) In nuclear emulsions the silver bromide grains are smaller in size and well separated compared to those in photographic emulsion. Hence, unlike photogr aphic emulsions, nuclear emulsions can be used for registering individual events.

iii) Nuclear emulsions are quite insensitive to light.

The composition of the elements silver, bromine, iodine, hydrogen, carbon, nitrogen, oxygen and sulfur present in nuclear

emulsions can vary depending upon the make and the specific use. In addition to these, it is possible to load nuclear emulsions with other elements like lithium, boron, bismuth and uranium for specific studies.

An ionising particle passing through nuclear emulsion leaves a track containing a number of developable silver bromide grains. Emulsions with the smallest grain size are sensitive only to densely ionising particles like fission fragments while those with coarse grains can register tracks of α-particles, protons, mesons and electrons also. Thus, a proper choice of grain size allows a discrimination between various particles.

The ranges or path lengths of ionising particles in nuclear emulsion, after development, can be measured using an optical microscope. The development of nuclear emulsions differ considerably, in many respects, from the techniques used for developing photographic emulsions mainly because nuclear emulsions plates are very thick and contain large quantities of silver. For thick emulsion plates, which are used particularly in high energy studies, the "temperature method" of **Dilworth** *et al.*[33] is particularly useful for obtaining uniform development of the whole emulsion without overdeveloping the outer layer. In this method, nuclear emulsion plates are first soaked in the developer solution for a long time at a temperature low enough to prevent the development process. Subsequently, the temperature is raised whereupon development proceeds uniformly throughout the emulsion.

In using nuclear emulsions for range measurement, special precautions have to be taken to see that there is not even the slightest distortion of gelatin due to the development process. Also, under extreme experimental conditions, the composition of the emulsions may change and proper corrections have to be applied to the measured ranges.

The energies of the ionising particles can be obtained from their ranges in nuclear emulsions using suitable range-energy relations. Though a number of range-energy relations have been developed, they lack general applicability, and in many cases require arbitrary corrections. A part of the present work is concerned with the development of general range-energy relations for heavy ions in complex media, including nuclear emulsions and is discussed in detail in Chapter 3.

4.4 SECTIONING TECHNIQUES

The measurement of ranges of heavy ions like fission products, which are of the order of a few microns in a given catcher, is not an easy task. To obtain proper range distributions sufficient data must be available and it is necessary to know concentrations per layer in depth increments of fractions of a micron. Though a large number of techniques have been developed for making such measurements the ones involving the removal of thin layers from the surface of the catcher coupled with the measurement of implanted atoms removed or remaining have proved the most successful.

4.4.1 Chemical Dissolution

In this method suitable chemical etchants are used for removing thin layers from the surface of the catcher by chemical dissolution. The method has been used in the study of the range profiles in sodium chloride and potassium bromide[34] and in GaAs.[35] The preferential etching rate on different crystallographic faces of the single crystal, at grain boundaries, dislocations, and, infact, at any point where local structure differs from the matrix, as for example, the implanted site, is a major disadvantage of this method. These difficulties, however, may not arise if amorphous catchers are used.

4.4.2 Anodic Oxidation / Chemical Dissolution

In 1960 Davies et al.[36] developed a novel peeling technique which has been responsible for much of the progress that has been achieved during the succeeding years in the study of range profiles, particularly of low energy ions. In this method the speciman is made the anode of an electrolytic cell and anodized to a known thickness of oxide layer. The thickness of the oxide layer is controlled by the voltage applied. The oxide layer is subsequently selectively dissolved using suitable solvents. Though undoubtedly the most sensitive and reproducible, it is at present limited to silicon,[37-39] aluminium,[36] tungsten,[40] gold,[41] molybdenum[42] and indium antimonide.[43] The limitation is not so much due to the difficulty in anodizing but in finding proper chemicals which selectively dissolve the oxide layer

without attacking the metal.

4.4.3 Corrosive Film / Chemical Dissolution

This method is based on the observation that when soft metals are immersed in an organic solvent containing halogen, a corrosive film is formed on the surface of the metal. This film can be selectively dissolved by chemicals which form complexes with metal halides. Andersen and Sørensen[44] have made range studies in copper, silver and gold using this method.

4.4.4 Mechanical Polishing

This technique has been used to measure range profiles in a wide variety of materials.[45] The main disadvantages of this method is that the deformations introduced in the specimen due to mechanical abrasion can result in anomalously shortened ranges. Nonetheless, the universal applicability compensates for this drawback.

4.4.5 Low Energy Ion Sputtering

The ejection of atoms from the surface of the material bombarded with energetic ions is known as sputtering. In principle, this method is applicable to all materials, but in practice, it is very sensitive to changes in crystal structure. Since the sputtering rates are different for different substances there is a possibility of the implanted atoms being sputtered out at a faster or slower rate than the matrix. Of more concern in range profile studies is that in materials damaged by ion implantation,

where the damage profile changes along the path, a continuous, but nonuniform change in sputtering rates through the range profile is likely. Not withstanding these drawbacks, the technique has been used by Lutz and Sizmann,[46] and by Pöhlaue *et al.*[47] for the measurement of range profiles in copper and gallium arsenide, respectively.

4.4.6 Electrolytic Dissolution

It has been well known that metals can be quantitatively dissolved as the anode of an electrolytic cell. However, there have been no attempts to use this technique for range measurement. In the present work, differential ranges of the fission products ^{140}Ba, ^{95}Zr and ^{89}Sr (from ^{235}U fission) in copper have been measured using this technique. The experimental procedure is discussed in detail in Chapter 5.

CHAPTER 5

COULOMETRIC METHOD OF RANGE MEASUREMENT

5.1 INTRODUCTION

Fission products from the thermal neutron induced fission of ^{235}U, after collimation, were allowed to penetrate a copper foil at right angles to its surface. Thin layers of accurately known thicknesses were then electrolytically dissolved out from the catcher foil. The thickness of the layers could be controlled by varying the duration of electrolysis and the current strength. The fission products whose range was to be measured was separated by radiochemical methods from the electrolyte after the dissolution of each layer. The range was obtained from a plot of the activity of the radioactive fission product in each layer against the depth at which the layer is situated.

5.2 TARGET PREPARATION

For accurate differential range measurements 'thin' targets are required so that there is negligible energy-loss of the fission product in the target material itself.

Thin targets of uranium can be obtained by its electrodeposition as hydrous oxide at the cathode.[48] The electrolytic cell is shown in Fig. 5.1. It consists of a glass cylinder G, ~3 cm in diameter and ~6 cm in height, with a flange at the lower end. The copper foil C, ~(2 cm x 2 cm) in area, on which uranium hydroxide is to be deposited is placed on a copper disc D. A copper wire is soldered to D for making electrical contact. The area of the deposit on the copper foil C which acts as the cathode was controlled by means of a teflon disc T, having a punched out hole of 1.5 cm diameter. The flange of G rests on T and is held in position tightly with the help of metal rings F, F' and screws which make the lower part leak-proof. The copper disc is insulated from the lower metal ring by mica. The platinum disc P, ~2 cm in diameter, acts as the anode.

The electrolyte consisted of equal volumes of 0.2 M perchloric acid and 0.15 M ammonium formate. To about 20 ml of the electrolyte in the electrolytic cell 0.5 ml of a dilute nitric acid solution of uranyl nitrate (containing ~200 μg of uranium enriched in ^{235}U (~60%)) was added. The anode and the cathode were about 2 cm apart. Electrolysis was carried out at room temperature (~25°C). A current density of ~50 milliamperes

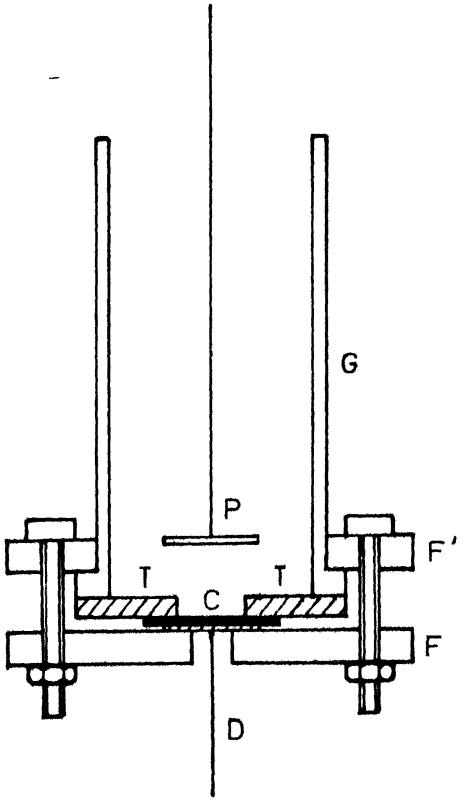

Fig. 5.1 Electrodeposition Cell

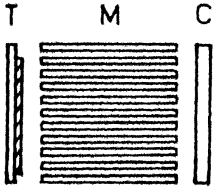

Fig. 5.2 Target assembly for irradiation.

per square centimeter of the cathode was maintained during electrolysis.

Under these experimental conditions anodic oxidation of the formate ion proceeds as follows:[48]

$$HCOO^- \longrightarrow CO_2 + H^+ + 2e^- ,$$

$$\text{at } E^\circ = 0.196 \text{ volt.}$$

This reaction produces half a hydrogen ion equivalent at the anode while the cathode reaction, involving hydrogen ion reduction, consumes one hydrogen ion equivalent per faraday of electricity. The net cell reaction causes the loss of half a hydrogen ion equivalent per faraday of electricity. The acidity of the electrolyte is slowly reduced and this causes the quantitative deposition of uranium hydroxide at the cathode because of the change in the pH. Electrolysis was carried out till approximately 75 μg of ^{235}U was deposited. After this the cathode with the uranium hydroxide deposit was removed, washed with distilled water and dried at 110°C.

5.3 TARGET ARRANGEMENT AND IRRADIATION

The deposited uranium on copper backing was then incorporated into the target assembly for the purpose of thermal-neutron irradiation. Figure 5.2 shows the target assembly. The uranium target on copper backing T, and the copper catcher foil C were

separated by the collimator M. The collimator was a 5 mm-thick aluminium block with about 100 parallel holes of 0.8 mm diameter in an area of ~2.5 square centimeter. This assembly was then wrapped in a pure aluminium foil, sealed in a glass container evacuated to a pressure of~5×10^{-6} meters of mercury, enclosed in water tight aluminium can and irradiated in the Apsara reactor, Bhabha Atomic Research Centre, Bombay, with a thermal neutron flux of the order of 10^{13} neutrons/cm^2sec. To get sufficient activity for good counting statistics irradiation was done for seven days after which the samples were allowed to "cool" for a few days so that the short-lived activation products decayed away and the samples could be handled with safety. The assembly was then opened and the catcher foils were subjected to the treatment described in the succeeding sections.

5.4 REMOVAL OF THIN LAYERS FROM THE CATCHER FOIL

Since copper has a low oxidation potential, thin layers could be removed from the copper catcher in an electrolytic cell. From the total quantity of electricity passed during electrolysis and the area of the anode in contact with the electrolyte the thickness of the layer dissolved can be calculated. If there is any purely chemical dissolution of the anode then corrections would have to be applied to the thickness calculated on the basis of purely electrochemical dissolution.

5.4.1 Electrolytic Cell

The electrolytic cell is shown in Fig. 5.3. It consists of a rectangular perspex chamber of dimensions 2 x 3 x 5 cm. The copper catcher foil from which thin layers are to be dissolved acts as the anode. The cathode consists of two identical copper strips having the same dimensions as the anode and mounted symmetrically on either side of the anode at a distance of ~1.5 cm from each other. The smaller the distance between the anode and the cathode compared to their own dimensions, the more uniform would be the electrical field between them resulting in more uniform dissolution of the anode surface. The anode and the cathode foils are fixed rigidly on a perspex frame so that during the removal of successive layers the geometry of the electrodes could be kept unaltered.

A Sargent coulometric current source, model-IV (supplied by E.H. Sargent and Co., U.S.A.) was used to obtain a constant current of precisely known strength for electrolysis. Six predetermined constant currents in the range of 4.825 milliampers to 193.0 milliampers could be selected. The timer which measures time in $\frac{1}{10}^{th}$ of a second is automatically switched on when the cell current is applied. The cell resistance of~250 ohms was in the specified range for which current regulation was $\pm$0.1 per cent.

5.4.2 Choice of Electrolyte

A 10% solution of sodium nitrate in 0.5 N nitric acid was used as the electrolyte. The choice of this electrolyte was

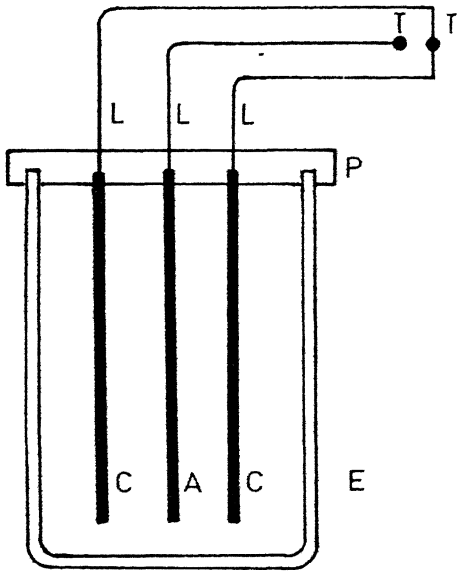

C CATHODE

A ANODE (CATCHER FOIL)

E PERSPEX CELL

P PERSPEX FRAME

L COPPER LEADS

T CONSTANT CURRENT SOURCE TERMINALS

Fig. 5.3 Electrolytic Cell

based on the following considerations:

A. Current Efficiency: The current efficiency of the electrolyte is one of the most important aspects that has to be taken into consideration in any constant current coulometric experiment. The current efficiency of the above electrolyte was studied beforehand as described below:

In the electrolytic cell a platinum wire was used as the cathode, the other electrode being a thin copper strip. Electrolysis was carried out for a short duration (~3 seconds) using a constant current of 4.825 milliampers. From the quantity of the electricity passed the quantity of copper expected to be deposited on the cathode was calculated on the basis of Faraday's law of electrolysis. The actual amount of copper deposited was determined spectrophotometrically by the dithizone[49] method as follows:

Calibration curve- A 0.01% copper solution was prepared by dissolving 0.1969 g of uneffloresced crystals of copper sulfate ($CuSO_4.5H_2O$) in 500 ml of 0.1 N sulfuric acid. From this solution weaker standards could be prepared by dilution with 0.1 N sulfuric acid. 10 ml of standard solution was taken in a small (50 ml) separatory funnel. 0.001% dithizone solution in carbon tetrachloride was delivered in small quantities from a microburette, shaking well the contents of the separatory funnel after each addition. The quantity of dithizone used was sufficient (i.e., slightly in excess) to extract the copper completely as copper dithizonate into carbon tetrachloride. This was indicated

by the change in the color of the final solution from that of pure copper dithizonate (red-violet). The exact volume of dithizone solution used was noted.

A few drops of carbon tetrachloride was allowed to flow out of the funnel to displace any aqueous solution in the bore of the stop-cock and the stem was dried with filter paper rolled around a glass rod. The copper dithizonate solution was then delivered into the quartz cell and the per cent transmittancy, T, of the solution was determined at 510 nm using spectronic-20 colorimeter (Bauseh & Lomb Optical Co., U.S.A.). The procedure was repeated with different standard solutions of copper. The calibration curve is shown in Fig. 5.4 in which $\log_{10}(1/T)$ is plotted against the concentration of copper (μg/l).

Determination of the Weight of Copper Deposited on the Cathode - The copper deposited on the platinum cathode was dissolved in dilute nitric acid (2 N HNO_3). The solution was evaporated to dryness and heated strongly to remove the oxides of nitrogen completely. The residue was dissolved in 5 ml of 0.1 N sulfuric acid. The whole of this solution was then shaken with 0.001% dithizone solution in a 50 ml separatory funnel as described before to extract copper completely into carbon tetrachloride as copper dithizonate. The exact volume of dithizone solution used was noted. The copper dithizonate solution was suitably diluted and the transmittancy was determined at 510 nm. The concentration of copper solution was obtained from the calibration curve

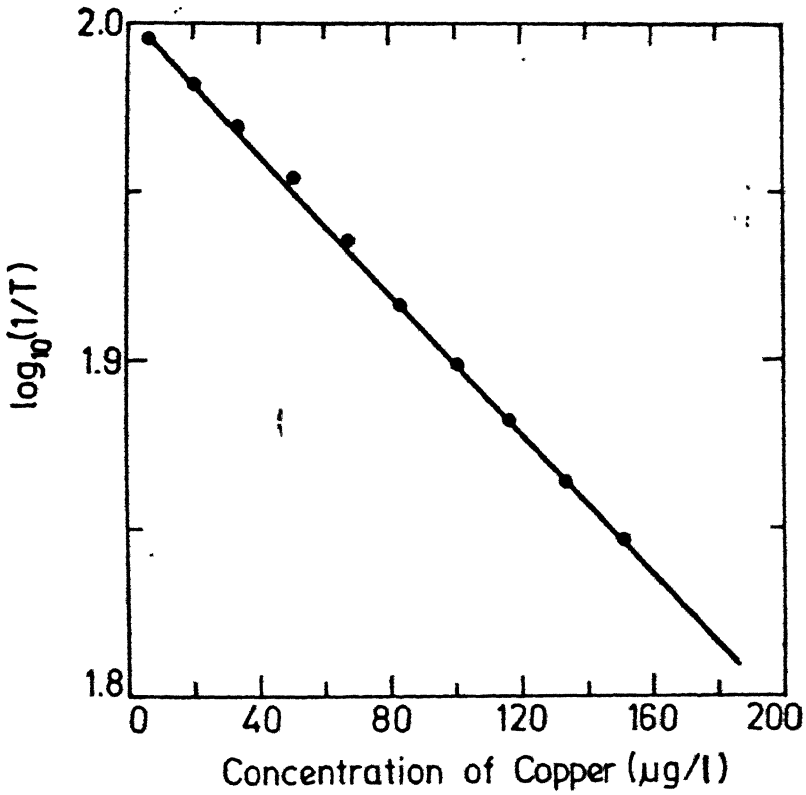

Fig. 5.4 Calibration curve.

and from this the weight of copper deposit was calculated. From the values given in Table 5.1 it can be seen that the current efficiency of the electrolyte can be taken to be 100% without introducing significant errors in range measurement.

B. Chemical Dissolution of Copper: The coulometric current source gives the total quantity of electricity passed during electrolysis and hence the amount of the anode material that has been dissolved electrolytically. If there is any purely chemical dissolution it is essential to account for it in calculating the thickness of the layers dissolved out. The following experiment was performed for this.

The copper anode was weighed accurately and the electrolysis was carried out for a known duration of time, approximately one hour. The loss in weight of the anode after electrolysis gave the weight of copper that had gone into solution both due to electrolysis and any possible chemical etching. As the current efficiency of the electrolyte had been found to be 100 per cent, the weight of copper dissolved electrolytically could be calculated from the quantity of electricity passed. Any difference between these two weights should give the weight of copper that had gone into solution due to purely chemical dissolution, and knowing the duration of electrolysis the rate of chemical attack could be calculated. Table 5.2 gives the experimental results. Since the difference in weights is within the limit of weighing accuracy (all weighings were done using a

Table 5.1

Comparison between the weights of copper deposit determined by the dithizone method (M_S) and that calculated using Faradays law of electrolysis (M_F)

Volume of dithizone solution used (ml)	Volume of copper dithizonate diluted to 10 ml (ml)	Per cent transmittancy of the diluted solution, T	log (1/T)	M_S (μg)	Total quantity of electricity used for electrolysis (microfaradays)	M_F (μg)
15.0	2.0	86.0	1.9345	4.950	0.155	4.925
13.6	2.0	85.5	1.9320	4.556	0.145	4.597

Table 5.2

Comparison between the weights of copper dissolved from the anode as determined by weighing and that calculated using Faraday's law of electrolysis

Total quantity of electricity passed (μF)	Wt. of the anode material expected to dissolve (mg)	Wt. of the anode before electrolysis (g)	Wt. of the anode after electrolysis (g)	Loss in wt. of the anode material (mg)
231.65	7.36	2.91238	2.90501	7.37
313.10	9.95	2.90501	2.89491	10.10

balance which can weigh down to 0.01 mg) no corrections for chemical attack was deemed necessary in calculating the thickness of the layers dissolved.

C. Ease of Chemical Separation of Fission Products: Since the electrolyte contains only sodium nitrate and nitric acid separation of fission products from it after electrolysis could be done easily using well tested methods available in literature with only minor modifications if, at all, required.[50, 51, 52]

5.4.3 Anodic Removal of Thin Layers from the Copper Catcher

The electrolytic cell was set up as described in Sec.5.4.1 with copper catcher foil (5x1.5 cm) as the anode. 15 ml of the

electrolyte was added to the cell covering the anode to a height of approximately 2.5 cm. Electrolysis was carried out for an accurately known duration of the order of 100 seconds. The duration of the electrolysis was chosen by taking into consideration the theoretical range of the fission product so that practically all the fission product activities could be dissolved out in about 35 layers of catcher in order to obtain a good differential range curve. The current was maintained constant at 48.25 milliamperes corresponding to a current density of approximately 10 milliamperes/cm^2 of the anode area. After each electrolysis the electrodes were carefully washed with demineralized water which was collected inside the cell. The solution in the electrolytic cell containing the fission products from the dissolved layer was transferred to a labelled 50 ml centrifuge tube. The electrolytic cell was washed with demineralized water and the washings were added to the same centrifuge tube. Electrolysis was repeated 35-40 times as described above and the solutions containing the fission product from each layer were stored separately in labelled 50 ml centrifuge tubes. The fission products whose ranges are to be determined were then separated from the above solutions radiochemically as described in the next section.

5.5 RADIOCHEMICAL SEPARATION OF FISSION PRODUCTS AND COUNTING

Radiochemical separations were done by "carrier" procedures in which milligram amounts of the elements of interest are added

at the beginning of the procedure. Since the amount of inactive carrier added is known, a determination of the amount present at the end of separation gives the chemical yield of the separation process and an appropriate correction is applied to the observed radioactivity to obtain the actual activity. To achieve good radiochemical purity one has to resort to repeated purification involving several precipitation and scavenging operations. Also, the procedures are often quite time-consuming. Taking these factors into consideration, it was advantageous to choose fission products with reasonably long half life and high fission yield. The fission products chosen for study in this work are given in Table 5.3 along with their half-life and cumulative yield which represents the probability of formation in fission of a nuclide of given mass number after prompt and delayed neutron emission and the decay of its short-lived precursor nuclides.

Table 5.3

Half -life and the cumulative yields for fission products chosen for range measurements

Fission product	Half-life (days)	Cumulative yield (%)
$^{140}_{56}Ba$	12.8	6.25
$^{95}_{40}Zr$	65.0	6.53
$^{89}_{38}Sr$	51.0	4.73

5.5.1 Barium-140

Barium can be separated from the other fission products by the specific precipitation at low temperature as $BaCl_2.2H_2O$ by means of concentrated hydrochloric acid- ethyl ether mixture. The procedure outlined below, which is similar to that developed by Glendenin,[50] consists of three precipitations as chloride, the first and second being followed by ferric hydroxide scavenging purification steps. The final precipitation of Barium as Barium chromate ($BaCrO_4$) was done in the presence of inactive strontium as hold-back carrier. The different steps involved in the separation procedure are described below:

i) 2 ml of barium chloride solution containing 20 mg of Ba^{2+} was added to the whole of the electrolyte solution containing the fission products from the layer dissolved from the catcher.

ii) Barium was precipitated as barium carbonate by adding saturated sodium carbonate solution in slight excess and centrifuged. The supernate was discarded.

iii) The barium carbonate precipitate was dissolved in 30 ml of ice-cold ether-hydrochloric acid mixture containing 1 volume diethyl ether and 5 volumes of concentrated hydrochloric acid, and cooled in ice with occasional stirring. White precipitate of barium chloride separates out. The precipitate was centrifuged and washed thrice with 5 ml portions of ice-cold ether-hydrochloric acid mixture.

iv) The barium chloride precipitate was dissolved in 5 ml of deionised water. 5 ml of Fe^{3+} scavenger, prepared by dissolving ferric chloride ($FeCl_3.6H_2O$) in very dilute hydrochloric acid was added. Ferric hydroxide was precipitated completely by adding concentrated ammonia dropwise with constant stirring and centrifuged.

v) Steps (ii), (iii) and (iv) were repeated with the supernate from step (iv).

vi) From the supernate in step (v) barium chloride was precipitated via steps (ii) and (iii).

vii) The barium chloride precipitate was dissolved in 5 ml of water. 20 mg of Sr^{2+} carrier, prepared by dissolving strontium chloride ($SrCl_2.2H_2O$) in water, was added to act as hold back carrier for strontium isotopes.

viii) The solution was neutralized with ammonia till just alkaline. 6N hydrochloric acid was added dropwise to make the solution just acidic to methyl orange. To this solution 1 ml of 6 M acetic acid and 2 ml of 6 M ammonium acetate were added. The contents were heated to nearly boiling and 1 ml of 1.5 M potassium chromate was added dropwise with stirring to precipitate barium chromate. Heating was continued for two minutes.

ix) A Whatman No. 42 filter paper disc, ~2.5 cm in diameter, was washed with distilled water and ethyl alcohol, dried at 110°C for 15 minutes, cooled to room temperature and weighed.

x) The barium chromate ($BaCrO_4$) precipitate was filtered on-to above filter paper disc in a Hirsch chimney. The precipitate was washed thrice with 5 ml portions of distilled water, thrice with 5 ml portions of ethyl alcohol, dried at 110°C for 15 minutes, cooled to room temperature and weighed. The chemical yield of barium chromate was ~70%.

xi) The barium chromate precipitate was mounted on an aluminium holder and the radioactivity was measured using a sharp low background beta proportional counter.

5.5.3 Zirconium-95

The separation of zirconium was done by using the procedure developed by Hahn and Skonieczny.[51] In this method, after the initial decontamination by scavenging with lanthanum fluoride in the presence of inactive zirconium (Zr^{4+}) carrier, zirconium is separated as insoluble barium fluozirconate. The purification of zirconium by two more precipitations as barium fluozirconate in acid medium is followed by its conversion to zirconium tetramandelate in which form it is weighed and counted. The separation procedure is given below:

i) To the electrolyte containing the fission products 2 ml of zirconium nitrate solution containing 5 mg of Zr^{4+} was added. The contents were transferred to a lusteroid tube. To this 0.5 ml 27 N hydrofluoric acid was added and mixed thoroughly.

ii) To the above solution 0.25 ml of lanthanum nitrate solution containing 10 mg of La^{3+}/ml was added, stirred well,

and centrifuged briefly. A second 0.25 ml of lanthanum nitrate solution was added and the precipitate was centrifuged down on top of the first precipitate. The supernate was decanted into another lusteroid tube.

iii) To the above supernate 1 ml of $Ba(NO_3)_2$ solution containing 50 mg of Ba^{2+} per ml was added, stirred well, and allowed to stand for a minute. The barium fluozirconate precipitate was centrifuged and the supernate discarded.

iv) To the lusteroid tube containing barium fluozirconate precipitate 2 ml of distilled water and 1 ml of saturated boric acid solution were added and stirred well. The precipitate was dissolved by adding 0.25 ml of concentrated nitric acid and heating on a waterbath. To the clear solution 0.5 ml of barium nitrate solution was added and mixed well. 0.25 ml of concentrated hydrofluoric acid was added to precipitate zirconium as barium fluozirconate. The precipitate was centrifuged and the supernate discarded.

v) Step (iv) was repeated with the precipitate.

vi) The precipitate from step (v) was suspended in 2 ml of water. 0.5 ml of saturated boric acid solution and 2 ml of 6 N hydrochloric acid was added and stirred well. The solution was made distinctly alkaline by adding 6 N sodium hydroxide with constant stirring. The zirconium hydroxide precipitate was centrifuged and the supernate was discarded.

vii) The zirconium hydroxide precipitate was dissolved in 3 ml of concentrated nitric acid and diluted to 6 ml. The

solution was transferred to a glass centrifuge tube. The lusteroid tube was rinsed twice with 1 ml portions of water and the washings were combined with the solution. 10 ml of saturated mandelic acid solution in water was added, stirred well and heated on a waterbath at 80°-90°C for about 20 minutes. Zirconium tetramandelate $Zr(C_6H_5CHOHCOO)_4$ precipitated out.

viii) The contents were filtered hot on-to a Whatman No. 42 filter paper disc, ~2.5 cm in diameter, which had been previously washed with water, ethyl alcohol and diethyl ether, dried at 50°C for 15 minutes cooled to room temperature and weighed. The precipitate was washed with 10 ml of 5% mandelic acid in 2% hydrochloric acid followed by three 5 ml portions of diethyl ether. The precipitate was dried for 15 minutes at 50°C, cooled to room temperature and weighed. The chemical yield of zirconium tetramandelate was~40%.

ix) The zirconium tetramandelate precipitate was then counted using a "sharp" low background beta proportional counter. Counting was done immediately after separation and no corrections have been applied to the contributions from the daughter ^{95}Nb which has a half-life of 35 days.

5.5.3 Strontium-89

The procedure for the separation of strontium from fission products was developed by Beaufait and Lukens.[52] Strontium is first precipitated as nitrate at low temperature by means of yellow fuming nitric acid. This is an excellent decontamination

step, the major impurity being barium. The strontium nitrate precipitate is purified by ferric hydroxide scavenging followed by quanitative precipitation of barium as chromate in the presence of inactive barium carrier. At this stage an oxalate precipitation followed by a nitrate precipitation will give the necessary radiochemical purity. The details of the method are given below:

i) To the sample solution containing the fission products 2 ml of strontium chloride solution containing 20 mg of Sr^{2+} was added. The solution was concentrated to a volume of about 2 ml.

ii) 20 ml of fuming nitric acid was added to the above solution and cooled in an ice-bath for 20 minutes with occassional stirring. The strontium nitrate precipitate was settled by centrifuging at low speed for about 10 minutes and the supernate was decanted off.

iii) The strontium nitrate precipitation was dissolved in 7 ml of distilled water 5 mg of Fe^{3+} solution was added to the above solution. Ferric hydroxide was precipitated completely by adding 6 N ammonium hydroxide dropwise with stirring. The ferric hydroxide scavenge was centrifuged and the char solution was transferred to another clean centrifuge tube. The ferric hydroxide scanvenge was washed by slurrying with 7 ml of 5% ammonium nitrate solution containing 2-3 drops of 6 N ammonium hydroxide and again centrifuged. The clear washings were combined with the above solution.

iv) 20 mg of Ba^{2+} carrier, prepared by dissolving barium chloride ($BaCl_2.2H_2O$) in water, was added to the above solution. The solution was neutralized with 6 N nitric acid, checking the pH with a pH paper. 1 ml of 6 M acetic acid and 2 ml of 6 M ammonium acetate were then added to the solution and it was heated nearly to boiling. Barium chromate was completely precipitated from this solution by adding 1 ml of 1.5 M potassium chromate dropwise with constant stirring. After centrifuging the clear supernate was transferred to another centrifuge tube.

To the above solution 2 ml of 6 N ammonium hydroxide was added and heated nearly to boiling. Strontium was precipitated as oxalate by adding 5 ml of saturated ammonium oxalate solution and centrifuged.

vi) The strontium oxalate precipitate was dissolved in 4 ml of 6 N nitric acid. 15 ml of yellow fuming nitric acid was added to it and cooled in ice for about 20 minutes with occasional stirring, and then centrifuged. The supernate was discarded.

vii) The strontium nitrate precipitate was dissolved in 10 ml of distilled water, neutralized with ammonium hydroxide and heated nearly to boiling. Strontium was precipitated as carbonate by adding 2 ml of 1 M sodium carbonate solution. Heating was continued for several minutes followed by cooling in ice for about 10 minutes.

viii) A Whatman No. 42 filter paper disc, $\sim$ 2.5 cm diameter, was washed with distilled water and ethyl alcohol, dried at 110°C

for 15 minutes, cooled to room temperature and weighed.

ix) The strontium carbonate precipitate was filtered on-to the above filter paper disc in a Hirsch chimney. The precipitate was washed thrice with 5 ml portions of water and thrice with 5 ml portions of ethyl alcohol. The precipitate was dried at 110^{o}C for 10 minutes, cooled to room temperature and weighed. The chemical yield of strontium carbonate was $\sim$60%.

x) The strontium carbonate precipitate was mounted on a aluminium holder and the radioactivity was measured in a sharp low background beta proportional counter.

5.6 RESULTS

After the counting the activity in the different layers the count rates were normalized to the same weight of the carrier and the same arbitrary initial time. The thickness of the layers dissolved out from the copper catcher and the normalized activity in them are shown in Tables 5.4, 5.5 and 5.6. Figures 5.5, 5.6 and 5.7 show the plot of the normalized count rate of different layers against the depth of the mid-point of the layer from the exposed surface. The well resolved, almost gaussian shaped, peaks allow the most probable ranges to be ascertained with good accuracy. The most probable ranges of ^{140}Ba, ^{95}Zr and ^{89}Sr are shown along with the full width at half maximum for the curves in Table 5.7.

Table 5.4

Thickness of the layers dissolved out from the copper catcher and the relative radioactivity (count rate normalized to 100% chemical yield and the same arbitrary initial time) of ^{140}Ba in them. A constant current of 48.25 milliamperes/second was used for electrolysis. The total area (both faces) of the copper catcher (anode) in contact with the electrolyte was 9.96 cm^2.

Layer No.	Duration of electrolysis (seconds)	Thickness of the layer dissolved ($\mu g/cm^2$)	Relative radioactivity (counts/minutes)
1	2	3	4
1*	100.5	178.2	
2	100.0	177.3	46.21 ± 1.29
3	100.1	177.5	56.56 ± 1.70
4*	100.0	177.3	
5	100.0	177.3	47.13 ± 1.26
6	100.0	177.3	27.13 ± 0.97
7	100.0	177.3	48.70 ± 1.43
8	99.9	177.1	
9	100.0	177.3	45.20 ± 1.38
10	100.0	177.3	
11	99.9	177.1	38.32 ± 1.03
12	100.1	177.5	31.99 ± 0.99
13	100.0	177.3	56.52 ± 1.69
14	100.4	178.1	65.56 ± 2.05
15	100.0	177.3	69.15 ± 2.02

...contd.

Table 5.4 (contd.)

1	2	3	4
16	100.1	177.5	95.89 ± 2.99
17.	99.9	177.1	108.29 ± 3.37
18.	100.0	177.3	128.38 ± 3.81
19	99.9	177.1	140.71 ± 4.34
20	100.0	177.3	158.22 ± 4.91
21.	100.2	177.6	171.57 ± 4.96
22	100.1	177.5	185.36 ± 5.59
23	100.1	177.5	187.65 ± 5.69
24	100.1	177.5	181.09 ± 5.51
25	100.2	177.6	165.96 ± 4.92
26	100.0	177.3	152.58 ± 4.74
27	100.1	177.5	130.37 ± 3.99
28	99.8	176.9	103.30 ± 3.56
29	100.0	177.3	95.10 ± 2.98
30	100.1	177.5	74.57 ± 2.22
31	99.9	177.1	59.69 ± 1.80
32	100.0	177.3	43.36 ± 1.35
33	100.1	177.5	33.52 ± 1.12
34	100.0	177.3	27.50 ± 0.83
35	99.9	177.1	20.50 ± 0.64
36	100.4	178.1	18.93 ± 0.57
37	100.0	177.3	15.33 ± 0.44
38	100.0	177.3	10.37 ± 0.32
39	100.2	177.6	8.99 ± 0.26

*These samples were spoiled during chemical separation.

Table 5.5

Thickness of the layers dissolved out from the copper catcher and the relative radioactivity (i.e., count rate normalized to 100% chemical yield and the same arbitrary initial time) of ^{95}Zr in them. A constant current of 48.25 mamp/sec was used for electrolysis. The total area (both faces) of the copper catcher (anode) in contact with the electrolyte was 6.08 cm^2.

Layer No.	Duration of electrolysis (seconds)	Thickness of the layer dissolved ($\mu g/cm^2$)	Relative radioactivity (counts/minutes)
1	2	3	4
1	150.0	391.8	39.73 ± 1.21
2	150.2	392.3	22.02 ± 0.66
3	130.1	355.9	20.32 ± 0.62
4	119.7	313.2	26.10 ± 0.78
5*	120.0	313.7	
6	120.0	313.7	15.66 ± 0.47
7*	120.1	313.7	
8	120.3	314.2	16.33 ± 0.48
9	119.7	313.2	
10	119.9	313.7	22.01 ± 0.65
11	120.0	313.7	30.58 ± 0.85
12	120.0	313.7	37.58 ± 1.17
13	120.0	313.7	42.59 ± 1.06
14	120.3	314.2	44.77 ± 1.14

....contd.

Table 5.5 (contd.)

1	2	3	4
15	120.0	313.7	89.37 ± 2.22
16	120.0	313.7	82.09 ± 2.24
17	119.8	312.9	101.39 ± 3.11
18	120.0	313.7	118.39 ± 3.70
19	120.0	313.7	117.86 ± 3.21
20	120.0	313.7	101.68 ± 4.01
21	120.0	313.7	75.82 ± 1.96
22	120.0	313.7	36.72 ± 0.84
23	120.0	313.7	32.57 ± 0.91
24	120.0	313.7	14.96 ± 0.46
25	119.7	313.2	8.97 ± 0.27
26	120.0	313.7	12.14 ± 0.38
27*	120.3	314.20	
28	120.1	313.7	2.16 ± 0.22

*These samples were spoiled during chemical separation

Table 5.6

Thickness of the layers dissolved out from the copper catcher and the relative radioactivity (count rate normalized to 100% chemical yield and the same arbitrary initial time) of ^{89}Sr in them. A constant current of 48.25 mamp/sec was used for electrolysis. The total area (both faces) of the copper catcher (anode) in contact with the electrolyte was 7.84 cm^2.

Layer No.	Duration of electrolysis (seconds)	Thickness of the layer dissolved ($\mu g/cm^2$)	Relative radioactivity (counts/minutes)
1	2	3	4
1	300.0	607.9	47.17 ± 1.49
2*	300.0	607.9	
3	200.0	405.2	51.67 ± 1.57
4	152.2	308.4	47.19 ± 1.48
5	148.0	299.5	49.34 ± 1.52
6	150.0	303.9	35.94 ± 1.02
7	150.2	304.3	31.90 ± 0.72
8	150.0	303.9	39.23 ± 1.23
9	150.0	303.9	48.64 ± 1.33
10	150.0	303.9	40.46 ± 1.00
11	150.0	303.9	48.90 ± 1.51
12	150.0	303.9	46.04 ± 1.36
13	150.1	304.1	55.59 ± 1.68
14	150.0	303.9	65.80 ± 2.05

.... contd.

Table 5.6 (contd.)

1	2	3	4
15	150.0	303.9	96.40 ± 2.97
16	150.0	303.9	130.70 ± 4.01
17	150.0	303.9	166.24 ± 4.95
18	150.0	303.9	183.35 ± 5.38
19	150.1	304.1	214.80 ± 6.45
20	150.0	303.9	190.41 ± 5.94
21	150.0	303.9	
22	150.2	304.3	113.81 ± 46.2
23	150.1	304.1	63.38 ± 1.08
24	150.2	304.3	16.16 ± 0.50
25*	149.8	299.9	
26	150.0	303.9	13.26 ± 0.39
27	150.0	303.9	11.18 ± 0.34
28*	150.0	303.9	
29	150.1	304.1	16.63 ± 0.49
30	150.8	305.6	11.63 ± 0.31
31	150.0	303.9	6.61 ± 0.21

*These samples were spoiled during chemical separation.

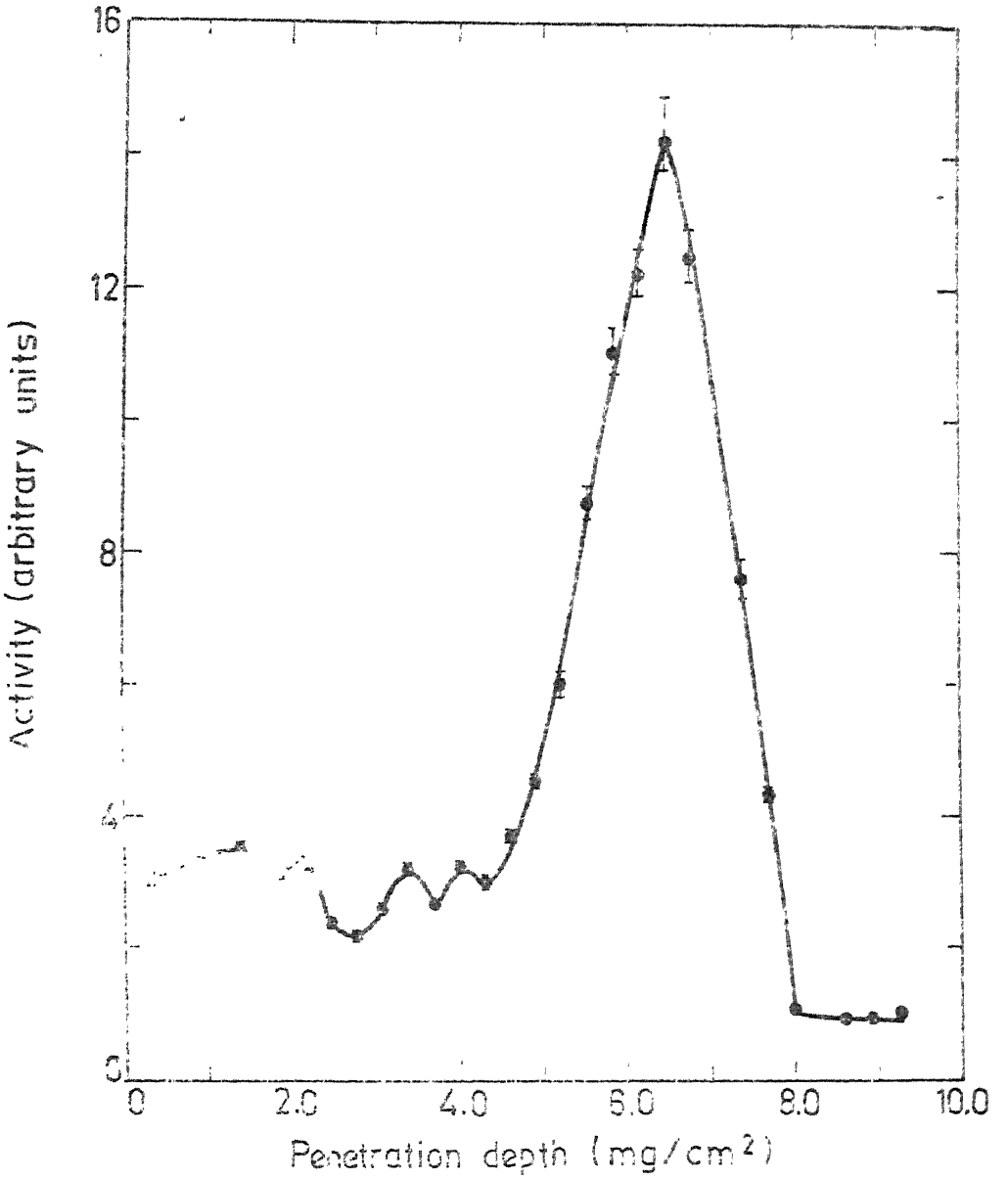

Fig. 5.5 Differential range distribution of the fission product ^{89}Sr in Copper.

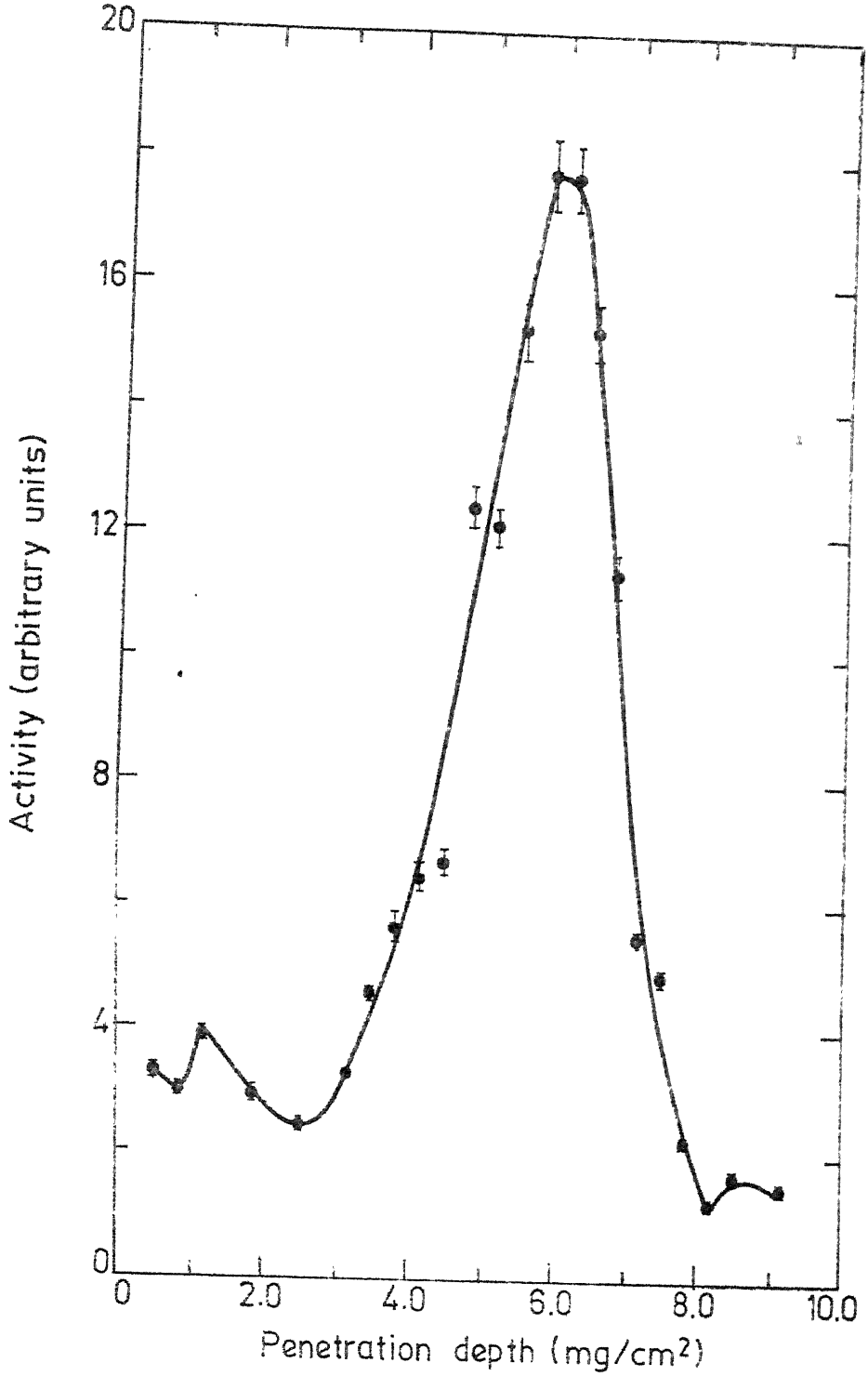

Fig. 5.6 Differential range distribution of the fission product ^{95}Zr in Copper.

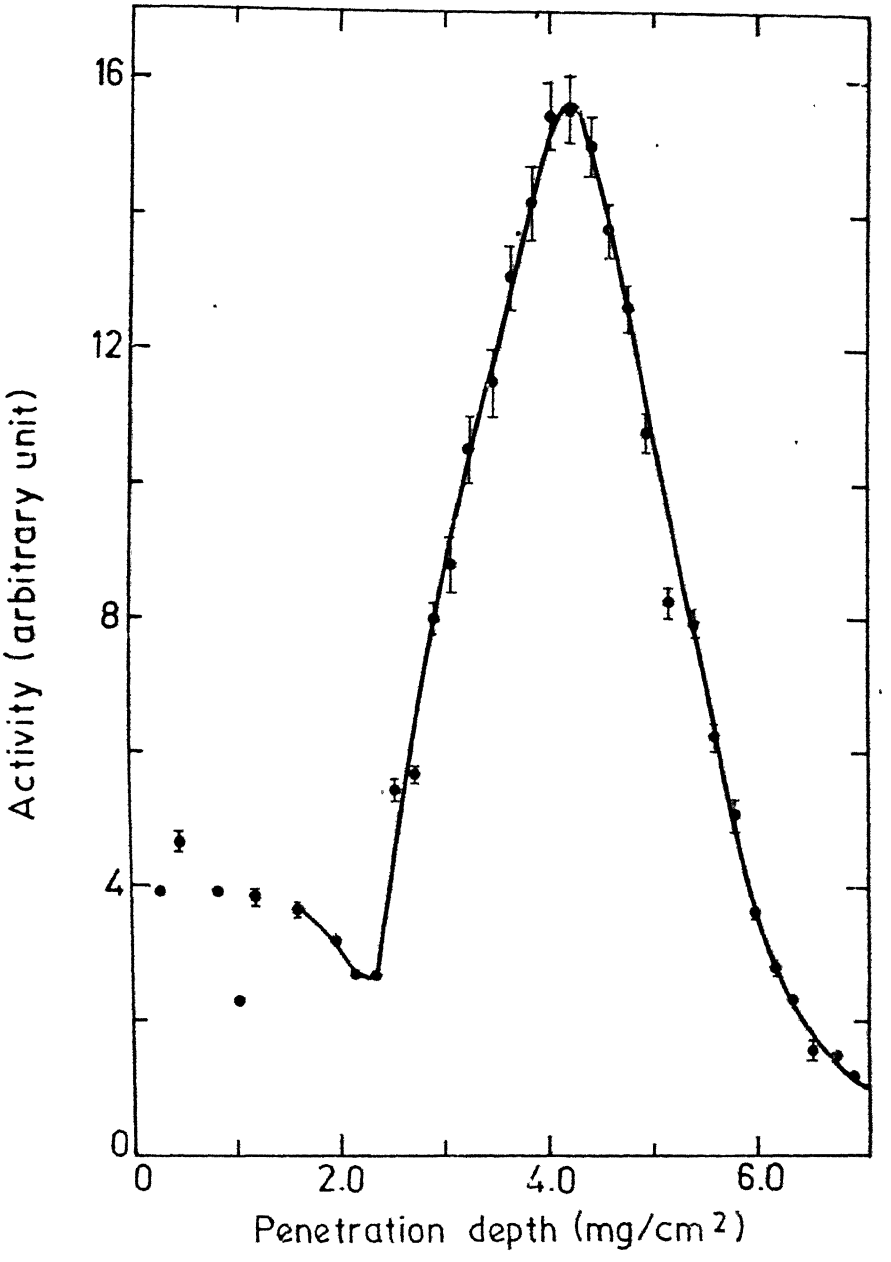

Fig. 5.7 Differential range distribution of fission product ^{140}Ba in Copper.

Table 5.7

The most probable ranges R_p (mg/cm^2) and the full width at half-maxima Ω (mg/cm^2) for the peaks

Fission Product	R_p (mg/cm^2)*	Ω (mg/cm^2)
$^{140}_{56}Ba$	4.080 ± 0.089	2.410
$^{95}_{40}Zr$	6.020 ± 0.157	2.320
$^{89}_{38}Sr$	6.330 ± 0.151	2.080

*The error in R_p corresponds to half the thickness of the layer dissolved out from the copper-catcher.

5.7 SOURCES OF ERROR IN THE MEASUREMENT

5.7.1 Determinate Errors in the Radiochemical Procedures

Some problems usually encountered in radiochemical work like determination of counting efficiency for the radiation and the standardization of the carrier solution did not appear in this study because only relative activities were needed. The primary sources of error to be considered lay in weighing, counting, radioactive impurity and scattering of beta radiation in the samples.

The samples were weighed using a balance which can read upto 0.01 mg. Since the samples weighed 60-80 mg the accuracy in weighing was of the order of 0.15%. The chemical procedures adopted have been shown to give adequate radioactive purity which was confirmed by careful monitoring of the decay of some of the samples. Since for the same fission product the chemical yield for the different samples did not differ appreciably no corrections were required for self absorption and back-scattering of the beta radiation.

5.7.2 Non-Uniformity in the Thickness of the Layers Dissolved from the Catcher Foil

The electric field between the parallel electrodes is not uniform, the lines of force being more crowded near the edges. Hence the rate of dissolution of the anode near the edges is higher than at the centre of the anode. The error in range measurement due to this effect was minimized by using electrodes

with large area and keeping the distance between them small to ensure a more uniform electric field between them.

5.7.3 Activation Impurities

Production of ^{140}Ba, ^{95}Zr and ^{89}Sr by neutron activation of impurities present in the catcher would cause considerable error in the range measurement of these fission products. To ensure that the nuclides whose ranges were measured were produced only by the fission of ^{235}U a 'blank run' was performed. Irradiations were carried out as described earlier but without the ^{235}U target. After irradiation the catcher foil was analysed for the activities present. The gamma ray spectra did not show any photopeaks for ^{140}Ba, ^{95}Zr and ^{89}Sr.

5.7.4 Collimation Angle

Because of the finite dimensions of the collimator holes, the fission products can penetrate the catcher surface at angles other than 90°. In the present work a 5 mm thick collimator having 0.8 mm diameter holes was used. The maximum deviation θ_{max} from 90° at which the fission product could penetrate the catcher surface, calculated using simple geometric considerations, was $\sim 9^{\circ}$. If all the fission products were to penetrate the catcher surface at $(90^{\circ} \pm \theta_{max})$ the measured ranges will be shorter by $\sim$1.2% from the true ranges. However, in actual measurements, the error would be smaller than this since all penetration angles between 90° and $(90^{\circ} \pm \theta_{max})$ are equally

probable. The ranges given in Table 5.7 have not been corrected for this effect.

5.8 DISCUSSION

5.8.1 Comparison with Other Methods

No data on ranges of the fission products ^{140}Ba, ^{95}Zr and ^{89}Sr in copper are available in literature. Hence, a comparison of the present measurement with other methods used for range measurements has not been possible. We could only compare our experimental values with the corresponding theoretical values calculated by means of a reliable range-energy equation which has been tested in the case of other media. This is given in the next section.

5.8.2 Comparison with Calculated Ranges

The ranges of the fission products can be calculated using the equation:[4]

$$R = \frac{A_1 A_2 \, (V_i - V_o)}{127.3 \; f(Z_2) \; [4.7622 \; f(Z_1)^{5/3} + f(Z_1)]} \qquad (5.1)$$

where R is the range in mg/cm^2 of the fission product of mass and atomic numbers A_1 and Z_1 respectively; A_2 and Z_2 are the mass and atomic numbers of the catcher material (stopping medium); V_i is the initial velocity of the fission product and $V_o = e^2/\hbar$; both V_i and V_o are expressed in units of 10^8 cm/sec. The f(Z) values are given by the equation:[4]

$$f(Z) = 0.28\ Z^{2/3} \quad \text{for } Z \leqslant 45.5\ , \tag{5.2}$$

$$f(Z) = Z^{1/3} \quad \text{for } Z > 45.5\ . \tag{5.3}$$

These f(Z) values were derived using the experimental ranges of fission products.

(a) Fission product velocities- For calculating the ranges of the fission products their initial velocities V_i are required. From the experimentally measured kinetic energies of the primary fission fragments the velocities of the fission products were calculated as follows. For the given fission product of mass number A_1 , the precursor fragment mass A_1' was calculated using the experimentally measured prompt neutron emission data of Apalin[53] et al. From the kinetic energies of the fission fragments obtained from Schmitt[54] et al., their velocities could be calculated. For thermal neutron induced fission of ^{235}U, the emission of prompt neutrons is almost isotropic. Therefore the emission of prompt neutron will not have significant efffect on the velocity of the fission fragment. Hence, the initial velocity of a fission product can be assumed to be the same as that of the corresponding precursor fragment. These velocities for the fission products ^{140}Ba, ^{95}Zr and ^{89}Sr are shown in Table 5.8.

(b) Effective nuclear charges of fission products- It should be noted that a particular fission product of mass number A_1 and nuclear charge Z_1 can be formed in two ways:

Table 5.8

The initial velocity (V_i) and the weighted average nuclear charge ($\bar{Z}_1$) for different fission products

Fission Product	Precursor Fragment Mass A_1'	V_i (in units of 10^8 cm/sec)	$\bar{Z}_1$
$^{140}_{56}Ba$	141.2	9.7081	54.36
$^{95}_{40}Zr$	96.35	14.2430	37.01
$^{89}_{38}Sr$	90.00	14.8035	35.00

i) Directly by the emission of prompt neutrons from the primary fission fragment. Prompt neutron emission from the highly excited primary fission fragment occurs in less than $\sim 10^{-13}$ second after the fissile parent nucleus undergoes scission.

ii) By the beta decay of the short-lived fission products of mass number A but atomic number $Z_i < Z_1$. The formation $^{140}_{56}Ba$, $^{95}_{40}Zr$ and $^{89}_{38}Sr$ in this way consists of the following chains:

$$^{140}_{56}Ba : \xrightarrow{\beta^-} {}^{140}_{54}Xe \xrightarrow{\beta^-} {}^{140}_{55}Cs \xrightarrow{\beta^-} {}^{140}_{56}Ba \xrightarrow{\beta^-}$$

$$^{95}_{40}Zr : \xrightarrow{\beta^-} {}^{95}_{36}Kr \xrightarrow{\beta^-} {}^{95}_{37}Rb \xrightarrow{\beta^-} {}^{95}_{38}Sr \xrightarrow{\beta^-} {}^{95}_{39}Y \xrightarrow{\beta^-}$$

$$^{95}_{40}Zr \xrightarrow{\beta^-}$$

$$^{89}_{38}Sr : \xrightarrow{\beta^-} {}^{89}_{35}Br \xrightarrow{\beta^-} {}^{89}_{36}Kr \xrightarrow{\beta^-} {}^{89}_{37}Rb \xrightarrow{\beta^-} {}^{89}_{38}Sr \xrightarrow{\beta^-}$$

Therefore, for any valid comparisons between the calculated and the experimentally measured ranges of a fission product of mass number A_1 and atomic number Z_1, it is necessary to replace Z_1 in Eq. (5.1) by a weighted average $\bar{Z}_1$ taking into account the contribution to its yield from all short-lived fission product which undergo beta decay into it. If the independent yield of a fission product of mass number A_1 and atomic number Z_1 is designated by $Y_{A_1}(Z_i)$, the fractional independent chain yield $I_{A_1}(Z_i)$ is given by

$$I_{A_1}(Z_i) = \frac{Y_{A_1}(Z_i)}{\sum_j Y_{A_1}(Z_j)} \qquad (5.4)$$

where the summation includes all fission products having mass number A_1. The weighted average nuclear charge $\bar{Z}_1$ for the fission product of mass number A_1 is given by

$$\bar{Z}_1 = \frac{\sum_{Z_i}^{Z_1} Z_i \; I_{A_1}(Z_i)}{\sum_{Z_i}^{Z_1} I_{A_1}(Z_i)} \qquad (5.5)$$

The fractional independent chain yields were obtained from Mukherji's prescription.[55] The effective nuclear charges calculated in this way for ^{140}Ba, ^{95}Zr and ^{89}Zr are shown in Table 5.8.

The ranges of the fission products ^{140}Ba, ^{95}Zr and ^{89}Sr calculated by using the effective nuclear charges $\bar{Z}_1$ and the initial velocities V_i in Eq. (5.1) are given in Table 5.9 and are compared with the corresponding experimental values. Since Eq. (5.1) for calculating ranges of fission products has been found to be quite reliable[4] the good agreement between the experimental and calculated values can be taken to be an indirect evidence of the relaiability of the present experimental technique.

Table 5.9

Comparison between the experimental (R_{expt}) and the calculated (R_{cal}) ranges

Fission Product	R_{expt} (mg/cm^2)	R_{cal} (mg/cm^2)
$^{140}_{56}Ba$	4.080 ± 0.089	4.121
$^{95}_{40}Zr$	6.020 ± 0.157	6.167
$^{89}_{38}Sr$	6.330 ± 0.151	6.454

CHAPTER 6

S U M M A R Y

The ranges of heavy ions in various elemental and complex media have been calculated. For doing this a set of stopping-power equations have been developed based on the earlier work by Bohr and that by Srivastava and Mukherji. An empirical method for calculating the mean ionization potential for all elemental media has been given. The "effective quantum number," $f(Z) = 0.3634\ Z^{0.555}$, which has been empirically introduced, seems to describe the velocity distributions of electrons in atoms with good accuracy, as is evident, although indirectly, from the good agreement between the calculated and experimental stopping-powers and ranges of heavy-ions both for light and heavy stopping media.

The ranges of the fission products ^{140}Ba, ^{95}Zr and ^{89}Sr from ^{235}U-fission have been measured in copper using an electrolytic technique. Though it has been well-known that metals can

be quantitatively dissolved as an anode of an electrolytic cell, it is for the first time that this idea has been used for range measurements, and the method seems to be quite accurate. The method can possibly be extended to the case of other metals, like Ag, Cr, Pb, Sn and Zr, having low oxidation potentials for measuring fission product or heavy ion ranges.

A P P E N D I X

The chemical composition of the "Standard" G-5 emulsion[25] has been used for obtaining the empirical formula for G-5 nuclear emulsion of density 3.815 g/cm^3.

Element	Weight, g/cm^3, of the emulsion	Number of gram-atoms / cm^3 of the emulsion	Number of atoms per atoms of Ag
Ag	1.8088	0.01676	1.000
Br	1.3319	0.01667	0.995
I	0.0119	0.00095	0.006
C	0.2757	0.02298	1.370
H	0.0538	0.05330	3.185
N	0.0737	0.00525	0.314
O	0.2522	0.01575	0.932
S	0.0072	0.00022	0.013

The Empirical formula of G-5 nuclear emulsion is, thus,

$AgBr_{0.995}\ I_{0.006}\ C_{1.370}\ N_{0.314}\ S_{0.013}\ H_{3.185}\ O_{0.932}$.

REFERENCES

1. N. Bohr, Philos. Mag., 25, 10 (1913).

2. H.A. Bethe, Ann. Phys., 5, 325 (1930).

3. N. Bohr, K. Danske. Vidensk. Selsk. Mat.-Fys. Medd., 18, No. 8 (1948).

4. S. Mukherji and B.K. Srivastava, Phys. Rev., B9, 3708 (1974).

5. B.K. Srivastava and S. Mukherji, Phys. Rev., A14, 718 (1976).

6. H.H. Heckman, B.L. Perkins, W.G. Simon, F.M. Smith and W.H. Barkas, Phys. Rev., 117, 544 (1960).

7. B.G. Harvey, Ann. Rev. Nucl. Sci., 10, 235 (1960).

8. R.D. Evans in "The Atomic Nucleus", p. 568 (Tata McGraw Hill Publishing Company Ltd., New Delhi, 1976).

9. F. Bloch, Ann. Phys., 16, 285 (1933).

10. J. Lindhard, M. Scharff and H.D. Schiøtt, K. Danske. Vidnsk. Selsk. Mat.-Fys. Medd., 33, No. 14 (1963).

11. H.A. Bethe and J.A. Ashkin in "Experimental Nuclear Physics," (Ed., E. Segre', Wiley, New York, 1953), Vol. 1, Ch. 2.

12. S. Mukherji, Phys. Rev., B12, 3530 (1975).

13. S. Mukherji and A.K. Nayak, Nucl. Inst. and Methods, 159, 421 (1979).

14. C.J. Bakker and E. Segre', Phys. Rev., 81, 489 (1951).

15. W.H. Barkas and M.J. Berger in "Studies in Penetration of Charged Particles in Matter" (National Academy of Science-National Research Council, Washington, D.C., 1964), Publ. 1133, p. 103.

16. H.H. Andersen, H. Sørensen and P. Vajda, Phys. Rev., 180, 373 (1969).

17. H. Sørensen and H.H. Andersen, Phys. Rev., B8, 1854 (1973).

18. N. Bohr and J. Lindhard, K. Danske, Vidensk. Selsk. Mat.-Fys. Medd., 28, 7 (1954).

19. P.G. Roll and F.E. Steigert, Nucl. Phys., 17, 54 (1960).

20. F.W. Martin and L.C. Northcliffe, Phys. Rev., 128, 1166 (1962).

21. J.R. Walton and E.L. Hubbard, quoted in L.C. Northcliffe, Ann. Rev. Nucl. Sci., 13, 69 (1963).

22. P.E. Schambra, A.M. Rauth and L.C. Northcliffe, Phys. Rev., 120, 1758 (1960).

23. D.E. Lea, in "Action of Radiations on Living Cells," (Cambridge Univ. Press, London, New York, 1946).

24. T. Brustad, Adv. Biol. Medd. Phys., 8, 161 (1962).

25. W.H. Barkas in "Nuclear Research Emulsions," Vol. I (Academic Press, New York and London, 1963).

26. P.G. Roll and F.E. Steigert, Nucl. Phys., 16, 534 (1962).

27. E. Segre' and C. Wiegand, Phys. Rev., 70, 808 (1946).

28. B. Finkle, E.J. Hoagland, S. Katcoff and N. Sugarman, Natl. Nucl. Energy Series, Div. IV, Book 1, p. 463 (McGraw Hill Publishing Co., New York, 1951).

29. N. Sugarman, M. Compas and K. Wielgoz, Phys. Rev., 101, 388 (1956).

30. J.B. Niday, Phys. Rev., 121, 1471 (1961).

31. J.M. Alexander and M.F. Gazdik , Phys. Rev., 120, 874 (1960).

32. M. Blau in "Nuclear Physics" (Eds. L.C.L. Yuan and C.S. Wu, Academic Press, New York and London, 1961), Vol. 5, Ch. 7.

33. C.C. Dilworth, G.P.S. Occhialini, R.M. Payne, Nature, 162, 103 (1948).

34. J.L. Whitton and Hj. Motzke, Can. J. Phys., 44, 2905 (1966).

35. J.D. Sansbury and J.F. Gibbons, Rad. Effects, 6, 269 (1970).

36. J.A. Davies, J. Friesen and J.D. McIntyre, Can. J. Chem., 38, 1526 (1960).

37. J.A. Davies, G.C. Ball, F. Brown and B. Domeij, Can. J. Phys., 42, 1070 (1964).

38. G.C. Dearnaley, J.H. Freeman, G.A. Gard and M.A. Wilkins, Can. J. Phys., 46, 587 (1968).

39. W. Pryborski, J. Roed, J. Lippart and L. Sarholt-Kristensen, Rad. Effects, 1, 33 (1969).

40. M. McCargo, J.A. Davies and F. Brown, Can. J. Phys., 41, 1231 (1963).

41. J.L. Whitton and J.A. Davies, J. Electrochem. Soc., 111, 1347 (1964).

42. M.R. Arora and R. Kelly, J. Electrochem. Soc., 119, 2 (1972).

43. M.A. Wilkins and G. Dearnaley, Proc. Conf. on Ion Implantation, Reading, Stevenage, England, Peter Perigrinus, p. 193 (1970).

44. T. Andersen and G. Sorensen, Rad. Effects, 2, 111 (1969).

45. J.L. Whitton, J. Appl. Phys., 36, 3917 (1965).

46. H. Lutz and R. Sizmann, Phys. Lett., 5, 113 (1963).

47. E. Pöhlau, H. Lutz and R. Sizmann, Z. Angew. Physik, 17, 404 (1964).

48. R. Ko, Nucleonics, 15(1), 72 (1957).

49. E.B. Sandell in "Colorimetric Determination of Trace Metals," Interscience Publishers, Inc., New York (1944).

50. L.E. Glendenin, NAS-NS Series, 9, paper 288, McGraw Hill Publishing Co., New York (1951).

51. R.B. Hahn and R.F. Skoniecczny, Nucleonics, 14, 56 (1956).

52. L.J. Beaufait Jr. and H.R. Lukens Jr. in "Handbook Radiochemical Analysis, Vol. II - Radiochemical Procedures," p. 122 (US Atomic Energy Commission, NP-5057 (Del), 1952).

53. V.A. Apalin, V.N. Gritsyuk, I.E. Kutikov, V.I. Lebedev and L.A. Mikaelian, Nucl. Phys., 71, 553 (1965).

54. H.W. Schmitt, J.H. Neiler and F.J. Walter, Phys. Rev., 141, 1146 (1966).

55. S. Mukherji, Nucl. Phys., A129, 297 (1969).